UNIVERSITY OF CALIFORNIA

Los Angeles

Maintenance of Interstitial Cells of Cajal for Intestinal Smooth Muscle Engineering

A dissertation submitted in partial satisfaction of the requirements for the degree Doctor of Philosophy in Bioengineering

by

Masae Kobayashi

2016

ABSTRACT OF THE DISSERTATION

Maintenance of Interstitial Cells of Cajal for Intestinal Smooth Muscle Engineering

by

Masae Kobayashi

Doctor of Philosophy in Biomedical Engineering

University of California, Los Angeles, 2016

Professor James C.Y. Dunn, Chair

Interstitial cells of Cajal (ICC) are the pacemakers that enable the oriented intestinal smooth muscle layers to contract rhythmically and autonomously. However, disruption of ICC networks has been reported in various intestinal motility disorders, which deteriorate the quality of life and life expectancy of a growing number of people in recent years. The key challenges in current intestinal smooth muscle engineering are the rapid loss of functional ICC and smooth muscle cells (SMC) in the culture. The objective of this study was to engineer functional intestinal smooth muscle with proper alignment and spontaneous rhythmic contraction by overcoming those obstacles. This was achieved by 1) developing orthogonally oriented scaffolds with aligned fibers for engineering intestinal smooth muscle *in vivo*; 2) identifying a reproducible culture system for *in vitro* maintenance of isolated ICC with pacemaker activity; and 3) engineering intestinal smooth muscle constructs with directional rhythmic contractions by implementing the functional ICC culture system into aligned scaffolds.

In summary, this research yielded reproducible practices using a simple feeder cell system for *in vitro* expansion of isolated ICC, which enabled the development of structurally desirable intestinal smooth muscle constructs exhibiting spontaneous membrane potential oscillations and contractions over 10 weeks *in vitro*. The demonstrated work not only contributed to the progress of intestinal tissue engineering, but also may provide valuable information for research in intestinal motility disorders, and for other types of visceral smooth muscle engineering including the bladder and vascular system.

Dissertation of Masae Kobayashi is approved.

Benjamin M. Wu

Timothy J. Deming

Atsushi Nakano

James C.Y. Dunn, Committee Chair

University of California, Los Angeles

2016

DEDICATION

To

Mom, my hero

Dad, my inspiration

I am who I am because of you

And

Professor Dunn, my guidance

I am where I am because of you

TABLE OF CONTENTS

ACKNOWLEDGEMENTS

I am very honored to be able to complete this dissertation under the guidance of Professor James Dunn. I would not be able to get where I am now if he was not my advisor. His generosity and patience provided the freedom for me to try my ideas, and to make mistakes in order to reach the possible solutions. His calmness always soothed me when I was facing difficulties. Moreover, his practicality never failed to set me back to accomplish my main goals. Although I felt shy and nervous while facing him until the end, I deeply respect him for who he is and how he presents himself. He is my "贵人," and I will remember him as a "正人君子" whom I encountered in my life.

I am thankful for all the suggestions and insights provided by Professor Benjamin Wu along this journey to enrich my research. I would like to thank Professor Min Lee, and my other dissertation committee members: Professor Timothy Deming and Professor Atsushi Nakano for their help to make this research more complete. I appreciate the kindness of Professor Benjamin Wu, Professor Min Lee and Professor Dino Di Carlo to give me the access to their facilities for this research to be completed. I would also like to thank Professor Timothy Deming, Professor Dino Di Carlo and Professor Stephanie Seidlits who hired me as their teaching assistant, which gave me the funding and the opportunities to prepare myself as a mentor.

Sincere thanks to all my current and former lab members. Especially to the following people: Hassan Khalil, thanks to him for conducting colonoscopic injections as part of *in vivo* study for my research. Francisco Lei, I cannot thank him enough for how much he supported me throughout my graduate school inside and outside the lab. I realized that he became one of my best friends who I should cherish a lifetime. Chris Walthers, thanks to him for all the advices he gave me and his willingness to help me with my research. Qianqian Wang, she inspired me to grow in many positive ways not only as a researcher but also as a person. I loved the jokes and small talks she used to tell me while we were working late nights in the lab. Steve Lin, I am glad that he became part of our lab after Chris Walthers graduated. I knew he would become "the next Chris," and he did it in no time by being always so helpful and nice to me and other lab members.

Lastly, I am grateful for all the supports from my parents throughout my life. I could live fully for myself all this time without any worries because they were always there for me when I needed them. Thanks to my little brother and Huimin Zhang for being there with me during the hardest time of my life. I am fortunate to have them all as my family.

Chapter 2 contains the following reused journal article:

> Kobayashi, M., Lei, N. Y., Wang, Q., Wu, B. M. & Dunn, J. C. Y. Orthogonally oriented scaffolds with aligned fibers for engineering intestinal smooth muscle. *Biomaterials* **61,** 75–84 (2015).

Included with copyright permission from: © 2016 Elsevier

*贵人: a most influential/important person in one's life, a savior

*正人君子: an upright gentleman, a man of moral integrity, a man of honor

VITA

Education

University of California, Los Angeles, Los Angeles, CA 90095
Henry Samueli School of Engineering and Applied Sciences
Bioengineering, Master of Science, Sep. 2010 – Dec. 2013

University of California, Berkeley, Berkeley, CA 94720
College of Engineering
Bioengineering, Bachelor of Science with High Honors, Dec. 2008

Teaching Experience

Teaching Fellow
Henry Samueli School of Engineering and Applied Sciences
University of California, Los Angeles, Jan. 2016 – Jun. 2016

Teaching Associate
Henry Samueli School of Engineering and Applied Sciences
University of California, Los Angeles, Jan. 2015 – Dec. 2015

Teaching Assistant
Henry Samueli School of Engineering and Applied Sciences
University of California, Los Angeles, Sep. 2013 – Dec. 2014

Publications

Kobayashi, M., Khalil, H.A., Lei, N. Y., Wang, Q., Wang, K., Wu, B. M. & Dunn, J. C. Y. Interstitial cells of Cajal enable engineering of rhythmically contracting intestinal smooth muscle. Submitted.

Kobayashi, M., Lei, N. Y., Wang, Q., Wu, B. M. & Dunn, J. C. Y. Orthogonally oriented scaffolds with aligned fibers for engineering intestinal smooth muscle. *Biomaterials* 61, 75–84 (2015).

Khalil, H. A. *et al.* Mouse model of endoscopically ablated enteric nervous system. *J. Surg. Res.* (2015). doi:10.1016/j.jss.2015.07.034

Yoo, S. Y. *et al.* M13 Bacteriophage and Adeno-Associated Virus Hybrid for Novel Tissue Engineering Material with Gene Delivery Functions. *Adv. Healthc. Mater.* (2015). doi:10.1002/adhm.201500179

Yoo, S. Y., Kobayashi, M., Lee, P. P. & Lee, S.-W. Early osteogenic differentiation of mouse preosteoblasts induced by collagen-derived DGEA-peptide on nanofibrous phage tissue matrices. *Biomacromolecules* **12,** 987–96 (2011).

Proceedings

Kobayashi, M., Khalil, H.A., Lei, N. Y., Wang, Q., Wang, K., Wu, B. M. & Dunn, J. C. Y. Stem Cell Factor Expressing Feeder Cells Enriches Intersititial Cells of Cajal for Engineering Functional Intestinal Smooth Muscle. Poster presentation at 4th Tissue Engineering and Regenerative Medicine International Society World Congress, Boston, MA, September 2015.

Kobayashi, M., Lei, N. Y., Wang, Q., Wu, B. M. & Dunn, J. C. Y. Orthogonally Oriented Scaffolds with Aligned Fibers for Engineering Intestinal Smooth Muscle. Oral and poster presentations at 16th Annual UC Systemwide Bioengineering Symposium, Santa Cruz, CA, June 2015.

CHAPTER ONE: INTRODUCTION

1.1 GASTROINTESTINAL TRACT DISORDERS

The intestine is part of our essential gastrointestinal (GI) tract, responsible for digestion, nutrient and water absorption and waste removal. Unfortunately, an increasing number of people are suffering from various intestinal disorders. According to Crohn's and Colitis Foundation of America, there are approximately 1.6 million Americans suffering from inflammatory bowel disease (IBD) in 2014. This is a 0.2 million increase in six years from 1.4 million IBD patients in 2008. Moreover, the American Cancer Society reported that the lifetime risk of developing colorectal cancer is about 5% and is the second leading cause of cancer-related deaths in the United States as of 2014. According to the International Foundation for Functional Gastrointestinal Disorders, children are diagnosed with common disorders like functional abdominal pain, chronic constipation, and irritable bowel syndrome at a rate similar to adults, which is 10% to 20%. In addition, Hirschsprung's disease, a congenital disorder associated with missing enteric nerve cells in part or all of the colon, occurs in about 1/5000 live births.

In some cases of the diseases listed above, surgery intervention is required. However, short bowel syndrome occurs in a patient when half or more of the bowel is removed during surgery or due to a birth defect. As a result, there may not be enough surface area in the bowel to absorb enough nutrients from food. Current treatments such as total parenteral nutrition (TPN) and transplantation have their own limitations. Patients who are dependent on TPN tend to experience severe liver complications while transplantation has common problems including donor scarcity, transplant rejection and life-long immunosuppression[1]. Therefore, engineering functional intestinal muscle tissues raises hope as an alternative therapeutic strategy for GI tract disorders.

1.2 INTERSTITIAL CELLS OF CAJAL (ICC): PHENOTYPES AND ROLES

The aligned smooth muscle layers of the GI tract move autonomously. Spontaneous electrical slow waves derived from pacemaker activity of the GI tract arrange contractile patterns into phasic contractions that are the root for peristalsis. GI muscles exhibit intrinsic pacemaker activity that does not depend on neural or hormonal inputs, while the degree of coupling between pacemaker activity and contractions is highly dependent on neural and other regulatory inputs. Basal spontaneous slow wave activity displays low amplitude contractions, and inhibitory or excitatory neural inputs modulate the amplitude[2].

ICC are a specialized group of cells involved in smooth muscle excitability that are mesenchymal in origin[3–5]. ICC play critical roles in visceral smooth muscles, including acting as electrical pacemakers to control phasic contractile activity and as mediators in motor neurotransmission. ICC have few contractile elements but contain abundant mitochondria, endoplasmic reticulum and caveolae for intracellular and extracellular calcium handling, and distinct membrane channels for their specialized functions as pacemakers and neuromodulators[6]. ICC have various morphologies in different locations of the GI tract. For example, ICC in the myenteric region (ICC–MY) are typically multipolar cells making frequent gap junctions with each other and forming an electrical network and closely associating with the enteric nervous system [7–10], whereas ICC within the muscles are long, thin, bipolar cells with few processes extending out to track along the axons of enteric motor neurons[7,8,10].

The binding of stem cell factor (SCF) to the receptor tyrosine kinase (Kit) induces a signaling pathway in ICC, which is critical for the normal development of ICC and rhythmic activity in the GI tract[11–15]. SCF stimulation of Kit is essential for ICC maintenance, as ICC vanish upon addition of neutralizing Kit antibody (ACK2) [14,16]. In addition, animals with

mutated Kit or SCF demonstrated disruption of the ICC-MY network in the small intestine and loss of the spontaneous electrical slow wave and contractile activity [11,17–20]. Moreover, ICC-MY display large amplitude electrical slow waves and are known for its pacemaker activity[21,22]. Recently, Ca^{2+} activated Cl^- channels (ano1) expressed on ICC were identified as the key conductance responsible for the pacemaker activity. Depolarization in ICC triggers slow waves with properties of Ca^{2+} activated Cl^- current. Slow waves propagate actively by depolarization-induced activation of low-threshold, voltage-dependent Ca^{2+} channels (ano1) that facilitate Ca^{2+} entry into ICC and induce Ca^{2+} release. These currents and slow waves were blocked by niflumic acid (a molecule that inhibits Cl^- channels)[23]. Transgenic mice with deactivated Tmem16a, a gene coding ano1, demonstrated normal morphological ICC networks but no slow waves[24]. Furthermore, ICC have the receptors required for transduction of neurotransmitter signals[25,26]. Prejunctional and postjunctional synaptic proteins exist at the interface between ICC and enteric varicosities[27] . Gap junctions exist between ICC and SMCs[28–30], though only few and small junctions are observed between ICC-MY and SMCs[31]. Activation of Ca^{2+} activated Cl^- channels in ICC generates inward currents leading to slow waves. Slow waves travel to SMCs forming cycles of depolarization that can activate Ca^{2+} channels and link slow waves to smooth muscle contractions[2]. ICC supply a pathway for the active propagation of slow waves, which enables the coordination of organ-level propagation of contractions leading to peristalsis[2]. Therefore, continuous networks of ICC are essential to engineer a GI tract with phasic electrical and mechanical activity.

Loss or disruption of ICC networks in GI muscles have been reported in a variety of intestinal motility disorders, including achalasia, chronic intestinal pseudoobstruction, Hirschsprung's disease, inflammatory bowel diseases, slow transit constipation, and diabetes[32–

[36]. Therefore, it is crucial to incorporate ICC in order to engineer functional intestinal smooth muscles.

1.3 FEEDER CELLS FOR ICC CULTURE

Isolated intestinal SMCs do not typically generate rhythmic electrical slow waves. Individual SMCs can possibly generate fast Ca^{2+} action potentials, but not the spontaneous slow waves in GI muscles. Conversely, isolated ICC generate spontaneous electrical rhythmicity similar to the electrical activity in intact GI muscles[23,37]. However, ICC only comprise less than 10% of total cells within intestinal smooth muscle layers and isolated ICC are hard to maintain in *in vitro* cell culture. ICC tend to lose their characteristic morphologies and Kit immunoreactivity after enzymatic digestion during the single cell isolation procedure. Although ICC have managed to grow and develop networks and electrical rhythmicity in cell culture, those dispersed ICC undergo extensive phenotypic changes within a few days, including the apparent loss of the ion channels responsible for the slow wave activity [23,38,39]. Since adequate Kit-SCF signaling is required for ICC proliferation and maturation, ICC were grown on fibroblast cell lines genetically engineered to express SCF. This study demonstrated that the number of Kit-positive ICC increased significantly when cultured with SCF expressing fibroblasts than with fibroblasts with no SCF expression[40]. However, all the ICC analyses were performed after only 48 hours in culture in this study because other types of cells overpopulated if cultured longer. Also, preparing SCF expressing fibroblasts by genetic modification may add another variable to the control in the culture system because the degree of SCF expression may vary from each preparation and may take a long time to acquire a stable and repeatable system. Therefore, it is beneficial to identify suitable SCF expressing feeder cells that are easily obtainable and

beneficial for *in vitro* ICC expansion. To my knowledge, no one has been able to expand functional ICC in *in vitro* culture for over a week with intact pacemaker activity. It will be crucial to the progress in intestinal smooth muscle engineering if suitable feeder cells can be identified for the *in vitro* expansion of functional ICC.

1.4 DISSERTATION OBJECTIVES AND SPECIFIC AIMS

The small and large intestines are part of our essential gastrointestinal (GI) tract and function to enhance the absorption of nutrients and water, and excretion of waste through synchronized peristalsis. However, many people are suffering from various intestinal disorders. For instance, over 1.5 million Americans are currently diagnosed with inflammatory bowel disease. As of 2014, colorectal cancer is the second leading cause of cancer-related deaths in the United States, and approximately 5% of people are at the risk of developing it. The essential GI motility can be disturbed due to disease, damage, surgical or obstetric trauma, and age. Some examples of congenital defects of GI motility are Hirschsprung's disease, intestinal pseudoobstruction, and achalasia[41]. However, currently available pharmacologic treatment and surgical correction does not provide a long term solution for those motility disorders. Therefore, tissue engineering is investigated in hope to regenerate the specific GI layers with proper architecture and functionality.

Aligned layers of smooth muscle in the GI tract move autonomously. However, this is not due to smooth muscle cells (SMCs) but cells called interstitial cells of Cajal (ICC). ICC are a specialized group of cells involved in smooth muscle excitability that are mesenchymal in origin[3–5]. ICC play critical roles in visceral smooth muscles, including acting as electrical pacemakers to control phasic contractile activity and as mediators in motor neurotransmission.

Loss or disruption of ICC networks in GI muscles has been reported in a variety of intestinal motility disorders. Extensive study has been performed to understand ICC physiology, yet no study has reported culturing ICC *in vitro* for tissue engineering purpose. Therefore, integration of the ICC population is an essential step in engineering functional intestinal smooth muscles.

The main challenges in current intestinal smooth muscle engineering are 1) *in vitro* expansion of functional ICC, 2) *in vitro* expansion of functional SMCs, and 3) the lack of structurally desirable implant with proper cell distribution and alignment. Dissertation objectives were set to address the challenges by completing the following three specific aims:

Aim 1: Develop orthogonally oriented scaffolds with aligned fibers for engineering intestinal smooth muscle *in vivo*. *Rationale.* Scaffold alignment has been used to induce cell alignment in previous studies [42–46]. In this aim, two-layer ePCL scaffolds with orthogonally aligned fibers were implemented to mimic tissue orientation of intestinal circular and longitudinal smooth muscle layers. The viability and alignment of cells infiltrated into the ePCL scaffolds *in vivo* was evaluated using ventral subcutaneous implantation into mice. At the conclusion of this aim, implants with desirable alignment that mimic the native intestinal muscle layers were developed.

Aim 2: Identify a reproducible culture system for *in vitro* maintenance of isolated ICC with pacemaker activity. *Rationale.* ICC isolated from small intestine are hard to maintain in *in vitro* cell culture. In this aim, optimization of the isolation, purification and identification techniques to acquire viable isolated ICC *in vitro* was accomplished initially. The effect of feeder cells to maintain ICC phenotype and the pacemaker activity *in vitro* was evaluated. At the conclusion of this aim, a reproducible protocol to *in vitro* culture primary isolated ICC with proper phenotypes and functionality was identified.

Aim3: Engineer intestinal smooth muscle constructs with directional rhythmic contractions by implementing the functional ICC culture system into aligned scaffolds.

Rationale. ICC plays an important role as pacemaker cells for intestinal smooth muscles to perform proper peristalsis. Loss of ICC in intestinal muscle layers often results in intestinal dysmotility. From the tissue engineering perspective, expanded ICC meet their ultimate role when they can restore the motility of SMCs. Using an optimized ICC culture system, intestinal SMC mixtures containing ICC, SMCs and neuronal cells were seeded onto aligned ePCL scaffolds. The effect of functional ICC to induce spontaneous rhythmic contractions of SMCs was evaluated. At the conclusion of this aim, smooth muscle constructs with rhythmic contractions and directionality was engineered.

In summary, this research 1) yielded reproducible practices for *in vitro* expansion of isolated ICC and 2) developed a structurally desirable implant that mimics intestinal smooth muscle layers 3) with spontaneous membrane potential oscillations and contractions.

1.5 REFERENCE

1. Donohoe, C. L. & Reynolds, J. V. Short bowel syndrome. *Surgeon* **8,** 270–9 (2010).
2. Sanders, K. M., Koh, S. D., Ro, S. & Ward, S. M. Regulation of gastrointestinal motility--insights from smooth muscle biology. *Nat. Rev. Gastroenterol. Hepatol.* **9,** 633–45 (2012).
3. Lecoin, L., Gabella, G. & Le Douarin, N. Origin of the c-kit-positive interstitial cells in the avian bowel. *Development* **122,** 725–733 (1996).
4. Young, H. M. Embryological origin of interstitial cells of Cajal. *Microsc. Res. Tech.* **47,** 303–8 (1999).
5. Young, H. M., Ciampoli, D., Southwell, B. R. & Newgreen, D. F. Origin of interstitial cells of Cajal in the mouse intestine. *Dev. Biol.* **180,** 97–107 (1996).
6. Sanders, K. A case for interstitial cells of Cajal as pacemakers and mediators of neurotransmission in the gastrointestinal tract. *Gastroenterology* **111,** 492–515 (1996).
7. Burns, A. J., Lomax, A. E., Torihashi, S., Sanders, K. M. & Ward, S. M. Interstitial cells of Cajal mediate inhibitory neurotransmission in the stomach. *Proc. Natl. Acad. Sci.* **93,** 12008–12013 (1996).
8. Burns, A. J., Herbert, T. M., Ward, S. M. & Sanders, K. M. Interstitial cells of Cajal in the guinea-pig gastrointestinal tract as revealed by c-Kit immunohistochemistry. *Cell Tissue Res.* **290,** 11–20 (1997).
9. KOMURO, T., SEKI, K. & HORIGUCHI, K. Ultrastructural characterization of the interstitial cells of Cajal. *Arch. Histol. Cytol.* **62,** 295–316 (1999).

10. Komuro, T. Structure and organization of interstitial cells of Cajal in the gastrointestinal tract. *J. Physiol.* **576,** 653–8 (2006).

11. Huizinga, J. D. *et al.* W/kit gene required for interstitial cells of Cajal and for intestinal pacemaker activity. *Nature* 347–349 (1995).

12. Klüppel, M., Huizinga, J. D., Malysz, J. & Bernstein, A. Developmental origin and Kit-dependent development of the interstitial cells of cajal in the mammalian small intestine. *Dev. Dyn.* **211,** 60–71 (1998).

13. Liu, L. W., Thuneberg, L. & Huizinga, J. D. Development of pacemaker activity and interstitial cells of Cajal in the neonatal mouse small intestine. *Dev. Dyn.* **213,** 271–82 (1998).

14. Maeda, H., Yamagata, A., Nishikawa, S. & Yoshinaga, K. Requirement of c-kit for development of intestinal pacemaker system. *Development* **116,** 369–375 (1992).

15. Wu, J. J., Rothman, T. P. & Gershon, M. D. Development of the interstitial cell of Cajal: origin, kit dependence and neuronal and nonneuronal sources of kit ligand. *J. Neurosci. Res.* **59,** 384–401 (2000).

16. Torihashi, S. *et al.* Blockade of kit signaling induces transdifferentiation of interstitial cells of Cajal to a smooth muscle phenotype. *Gastroenterology* **117,** 140–148 (1999).

17. Malysz, J., Thuneberg, L., Mikkelsen, H. & Huizinga, J. Action potential generation in the small intestine of W mutant mice that lack interstitial cells of Cajal. *The American journal of physiology* G387-99 (1996).

18. Mikkelsen, H. B., Malysz, J., Huizinga, J. D. & Thuneberg, L. Action potential generation, Kit receptor immunohistochemistry and morphology of steel-Dickie (Sl / Sl d) mutant mouse small intestine. *Neurogastroenterol. Motil.* **10,** 11–26 (1998).

19. Ward, S. M., Burns, A. J., Torihashi, S., Harney, S. C. & Sanders, K. M. Impaired development of interstitial cells and intestinal electrical rhythmicity in steel mutants. *Am. J. Physiol.* **269,** C1577-85 (1995).

20. Ward, S. M., Burns, A. J., Torihashi, S. & Sanders, K. M. Mutation of the proto-oncogene c-kit blocks development of interstitial cells and electrical rhythmicity in murine intestine. *J. Physiol.* **480,** 91–97 (1994).

21. Dickens, E. J., Hirst, G. D. & Tomita, T. Identification of rhythmically active cells in guinea-pig stomach. *J. Physiol.* **514 (Pt 2,** 515–31 (1999).

22. Kito, Y. & Suzuki, H. Properties of pacemaker potentials recorded from myenteric interstitial cells of Cajal distributed in the mouse small intestine. *J. Physiol.* **553,** 803–18 (2003).

23. Zhu, M. H. *et al.* A Ca(2+)-activated Cl(-) conductance in interstitial cells of Cajal linked to slow wave currents and pacemaker activity. *J. Physiol.* **587,** 4905–18 (2009).

24. Hwang, S. J. *et al.* Expression of anoctamin 1/TMEM16A by interstitial cells of Cajal is fundamental for slow wave activity in gastrointestinal muscles. *J. Physiol.* **587,** 4887–904 (2009).

25. Chen, H. *et al.* Selective labeling and isolation of functional classes of interstitial cells of Cajal of human and murine small intestine. *Am. J. Physiol. Cell Physiol.* **292,** C497-507 (2007).

26. Iino, S., Horiguchi, K., Nojyo, Y., Ward, S. M. & Sanders, K. M. Interstitial cells of Cajal contain signalling molecules for transduction of nitrergic stimulation in guinea pig caecum. *Neurogastroenterol. Motil.* **21,** 542–50, e12-3 (2009).

27. Beckett, E. a H., Takeda, Y., Yanase, H., Sanders, K. M. & Ward, S. M. Synaptic specializations exist between enteric motor nerves and interstitial cells of Cajal in the murine stomach. *J. Comp. Neurol.* **493,** 193–206 (2005).

28. Thuneberg, L. Interstitial cells of Cajal: intestinal pacemaker cells? *Adv. Anat. Embryol. Cell Biol.* **71,** 1–130 (1982).

29. Imaizumi, M. & Hama, K. An electron microscopic study on the interstitial cells of the gizzard in the love-bird (Uroloncha domestica). *Zeitschrift fur Zellforsch. und Mikroskopische Anat.* **97,** 351–357 (1969).

30. Gabella, G. & Blundell, D. Gap junctions of the muscles of the small and large intestine. *Cell Tissue Res.* **219,** 469–488 (1981).

31. Daniel, E. E. & Wang, Y. Gap Junctions in Intestinal Smooth Muscle and Interstitial Cells of Cajal. *Microsc. Res. Tech.* **47,** 309–320 (1999).

32. Rumessen, R. I. J. Interstitial Cells of Cajal in Human Gut and Gastrointestinal Disease. *Microsc. Res. Tech.* **47,** 344–360 (1999).

33. Sanders, K. M., Ordög, T. & Ward, S. M. Physiology and pathophysiology of the interstitial cells of Cajal: from bench to bedside. IV. Genetic and animal models of GI motility disorders caused by loss of interstitial cells of Cajal. *Am. J. Physiol. Gastrointest. Liver Physiol.* **282,** G747-56 (2002).

34. Burns, A. J. Disorders of interstitial cells of Cajal. *J. Pediatr. Gastroenterol. Nutr.* **45 Suppl 2,** S103-6 (2007).

35. Farrugia, G. Interstitial cells of Cajal in health and disease. *Neurogastroenterol. Motil.* **20,** 54–63 (2008).

36. Horváth, V. J. *et al.* Reduced stem cell factor links smooth myopathy and loss of interstitial cells of cajal in murine diabetic gastroparesis. *Gastroenterology* **130,** 759–70 (2006).

37. Langton, P., Ward, S. M., Carl, A., Norell, M. A. & Sanders, K. M. Spontaneous electrical activity of interstitial cells of Cajal isolated from canine proximal colon. *Proc. Natl. Acad. Sci.* **86,** 7280–7284 (1989).

38. Thomson, L. *et al.* Interstitial cells of Cajal generate a rhythmic pacemaker current. *Nat. Med.* **4,** 848–851 (1998).

39. Koh, S. D., Sanders, K. M. & Ward, S. M. Spontaneous electrical rhythmicity in cultured interstitial cells of Cajal from the murine small intestine. *J. Physiol.* **513,** 203–213 (1998).

40. Rich, A. *et al.* Local presentation of Steel factor increases expression of c-kit immunoreactive interstitial cells of Cajal in culture. *Am. J. Physiol. Gastrointest. Liver Physiol.* **284,** G313-20 (2003).

41. Chumpitazi, B. & Nurko, S. Pediatric gastrointestinal motility disorders: challenges and a clinical update. *Gastroenterol. Hepatol. (N. Y).* **4,** 140–8 (2008).

42. Ionescu, L. C. & Mauck, R. L. Porosity and Cell Preseeding Influence Electrospun Scaffold Maturation and Meniscus Integration In Vitro. *Tissue Eng. Part A* **19,** 538–547 (2013).

43. Ayres, C. *et al.* Modulation of anisotropy in electrospun tissue-engineering scaffolds: Analysis of fiber alignment by the fast Fourier transform. *Biomaterials* **27,** 5524–34 (2006).

44. Courtney, T., Sacks, M. S., Stankus, J., Guan, J. & Wagner, W. R. Design and analysis of tissue engineering scaffolds that mimic soft tissue mechanical anisotropy. *Biomaterials* **27,** 3631–8 (2006).

45. Reneker, D. H. & Chun, I. Nanometre diameter fibres of polymer, produced by electrospinning. *Nanotechnology* **7,** 216–223 (1996).

46. Li, W.-J., Mauck, R. L., Cooper, J. a, Yuan, X. & Tuan, R. S. Engineering controllable anisotropy in electrospun biodegradable nanofibrous scaffolds for musculoskeletal tissue engineering. *J. Biomech.* **40,** 1686–93 (2007).

CHAPTER TWO: ORTHOGONALLY ORIENTED SCAFFOLDS WITH ALIGNED FIBERS FOR ENGINEERING INTESTINAL SMOOTH MUSCLE

2.1 ABSTRACT

Controlling cellular alignment is critical in engineering intestines with desired structure and function. Although previous studies have examined the directional alignment of cells on the surface (x-y plane) of parallel fibers, quantitative analysis of the cellular alignment inside implanted scaffolds with oriented fibers has not been reported. This study examined the cellular alignment in the x-z and y-z planes of scaffolds made with two layers of orthogonally oriented fibers. The cellular orientation inside implanted scaffolds was evaluated with immunofluorescence. Quantitative analysis of coherency between cell orientation and fiber direction confirmed that cells aligned along the fibers not only on the surface (x-y plane) but also inside the scaffolds (x-z & y-z planes). Our study demonstrated that two layers of orthogonally aligned scaffolds can generate the histological organization of cells similar to that of in- testinal circular and longitudinal smooth muscle.

2.2 INTRODUCTION

In the small intestine, the inner circular smooth muscle layer is orthogonally oriented to the outer longitudinal smooth muscle layer, and the myenteric plexus is embedded between these layers. The arrangement of smooth muscle cells, neural cells and interstitial cells of Cajal within the intestinal smooth muscle is highly organized in order to coordinate peristalsis [1]. In other tissues such as the vasculature [2,3], myocardium [4], skeletal muscle [5], nervous system [6,7], and connective tissues [8,9], cellular alignment is also essential for their proper function. It is

therefore desirable to replicate the native microstructures and cellular alignment for tissue engineering constructs.

Electrospun scaffolds with aligned fibers have been explored for their suitability to align cells in many tissue engineering applications [5,10–13]. Various synthetic and biological polymers have been electrospun to fabricate scaffolds with desired fiber size and alignment [14,15]. These fibers replicate the length scale of elements in the native extracellular matrix and promote cellular differentiation and matrix production [16,17]. Aligned fibers can be fabricated by collecting elecrospun fibers on rotating mandrels, leading to controllable mechanical and structural anisotropy [5,12,18,19]. Among a variety of FDA approved polymers, poly(3-caprolactone) (PCL) is a promising material due to its biocompatibility, biodegradability and mechanical properties. Fibrous scaffolds composed of PCL are 10 times less stiff and stay elastic over a wider range, as compared to scaffolds made of poly(D,L-lactic- co-glycolic acid 50:50) [20]. Electrospun PCL (ePCL) scaffolds with aligned fibers were shown to enhance cellular alignment, matrix deposition, and increased tensile properties along the fiber direction when compared to similar scaffolds with randomly oriented fibers [5,21]. Such flexibility and controllable directionality of ePCL scaffolds make it a suitable choice for muscle tissue engineering.

Previous studies have examined the cellular alignment on the 2D surface (x-y plane) of cells in culture [2,5–9,22], but the alignment of cells inside 3D scaffolds *in vivo* has not been analyzed quantitatively. We hypothesized that a two-layer ePCL scaffold with orthogonally aligned fibers would generate 3D cellular alignment analogous to the intestinal circular and longitudinal muscle layers. In this study, we compared the cellular alignment in the x-z and y-z planes of implanted ePCL scaffolds made with either aligned or randomly oriented fibers.

2.3 MATERIALS AND METHODS

2.3.1 Electrospinning

11% (w/w) solution of PCL (Durect Lactel, Birmingham, AL) was made in hexafluoro-2-propanol (Acros Organics, Thermo Fisher Scientific, Waltham, MA). The solution was kept on a shaker overnight to obtain a homogenous polymer solution. The mandrel was wrapped with aluminum foil to ease the removal of the scaffold. The PCL solution was transferred to a plastic syringe fitted with an 18-gauge needle, and secured onto a syringe pump (Harvard Apparatus, Holliston, MA). The solution was infused at 2.5 ml/h onto a rotating mandrel collector with an outer diameter of 32 mm that was positioned 12-15 cm away from the needle tip. The electrical potential difference between the needle (i.e., polymer solution) and the grounded mandrel collector was produced by a high voltage power supply (Glassman High Voltage, High Bridge, NJ). Scaffolds comprised of aligned ePCL fibers were fabricated using a mandrel rotational speed of 3450 rpm and an applied voltage of 15 kV. Less-aligned, “random” ePCL fibers were produced using a mandrel rotational speed of 1725 rpm and applied voltage of 25 kV. After 0.5 ml of polymer solution had been dispensed from the syringe onto the rotating mandrel, the ePCL was carefully removed from the aluminum foil. Scaffolds were air-dried before laser cutting (Fig. 1A).

2.3.2 Scanning Electron Microscopy (SEM)

The surface morphology of ePCL scaffolds with aligned or random fibers was assessed using a Nova NanoSEM 230 (FEI, Hillsboro, Oregon). The scaffolds without conductive coating were mounted on the sticky conductive carbon tape (Ted Pella, Redding, California) on the top of

aluminum stubs (Ted Pella, Redding, California) and examined under SEM with an accelerating voltage of 10 kV at low vacuum mode.

2.3.3 Laser cutting

The ePCL scaffolds were constructed as fiber sheets with dimensions approximately 10 x 2.5 cm and thickness of 100-150 µm, based on the mandrel used. These fiber sheets were cut into rectangular 8 x 6.5 mm scaffolds using the VERSA LASER CUTTER 2.3 (Universal Laser Systems, Scottsdale, AZ) with vector mode, 5% power, 100x speed, and 1000 pulses/inch. Two types of scaffolds were obtained by setting the longer or shorter edge of the rectangle to be along the fiber direction (Fig. 1B). The scaffolds were sterilized in 70% ethanol for 30 min and washed several times with phosphate buffered saline (PBS).

2.3.4 Ethics statement

Animal usage complied with regulations set by the University of California, Los Angeles, Chancellor's Animal Research Committee and was approved as animal protocol number 2005-169. All efforts were made to minimize pain and suffering. Two mice strains were used for these experiments: C57BL/6-Tg(Actb-EGFP)1Osb/J ("GFP") (The Jackson Laboratory, Bar Harbor, ME) and wild type C57BL/6 (Charles River, Wilmington, MA).

2.3.5 Intestinal smooth muscle strips (SMS) isolation and culture

SMS were isolated from two 7 to 8-day-old GFP-positive C57BL/6 neonates using previously described methods [23–25]. The intestines were removed via a midline incision, and smooth muscle strips, containing both longitudinal and circular muscle layers, were gently teased from

the intestines using fine forceps and placed in Hank's Balanced Salt Solution without calcium and magnesium (Invitrogen, Carlsbad, CA) on ice. SMS were minced thoroughly using a scalpel. Approximately one-tenth of the SMS were seeded directly to each ePCL scaffold, which was coated with gelatin solution (attachment factor solution; Invitrogen, Carlsbad, CA) at 37°C for at least 30 min and briefly washed with PBS once in advance. SMS-seeded ePCL scaffolds were cultured at 37°C in a 5%CO_2 incubator in Knockout™ D-MEM supplemented with 15% FBS, 0.1 mM 2-mercaptoethanol, 0.1mM non-essential amino acids (NEAA), 2mM L-glutamine, and 1x antibiotic-antimycotic (all from Invitrogen, Carlsbad, CA). The medium was changed after 2 days to the same medium but without antibiotic-antimycotic. SMS-seeded ePCL scaffolds were incubated *in vitro* for approximately 3 weeks before implantation to allow infiltration of cells inside the scaffolds. The SMS-seeded sides of two ePCL scaffolds were connected together to form a two-layer scaffold with 10 μL of collagen gel (*PureCol*® EZ Gel, Advanced BioMatrix, San Diego, CA) right before implantation (Fig. 1E-H).

2.3.6 Scaffold Implantation

ePCL scaffolds with or without cells were implanted subcutaneously into syngeneic wild type adult C57BL/6 mice. Recipient mice were anesthetized with inhaled isoflurane and given a subcutaneous injection of 0.05 mg/kg buprenorphine. The abdomen was shaved, prepared, and draped sterilely. A ventral midline incision was made and skin flaps were raised laterally to create subcutaneous pockets. The ePCL scaffolds were sutured to the abdominal wall using 6-0 Prolene suture (Ethicon, Somerville, NJ), and the incision was closed using 3-0 silk suture (Ethicon). Recipient mice with SMS-seeded scaffolds were sacrificed approximately 4 days postoperatively while recipient mice with scaffolds without initial SMS seeding were sacrificed

approximately 2 weeks postoperatively. The explants were formalin-fixed and processed for histological evaluations.

2.3.7 Histology & immunofluorescence staining

In vivo explants were fixed and processed for paraffin embedding. Serial 5-µm sections were cut and adhered to glass slides; every third slide was stained with hematoxylin and eosin (HE). Unstained slides were prepared for immunofluorescence staining. Slides were de-waxed with xylene and rehydrated with serial dilutions of ethanol. Next, slides were incubated in a citric buffer (Biogenex, San Ramon, CA) for 15 min at 95-100°C and allowed to cool for 15 minutes in an over flowing water bath. *In vitro* cultures were fixed without histologic processing. After three washes with PBS, samples were treated with blocking buffer containing 5% normal goat serum (Vector Labs, Burlingame, CA), 0.1% Triton X-100 (Sigma) in PBS for 1 hour at 4°C. Samples were then incubated with primary antibodies against alpha smooth muscle actin (α-SMA) (1:250; Dako, Carpinteria, CA) and green fluorescent protein (GFP) (1:1000, Abcam, Cambridge, MA) diluted in blocking buffer overnight at 4°C. After two washes in PBS, samples were incubated in the dark with their corresponding secondary antibodies (goat anti-mouse Alexa Fluor 488, goat anti-rabbit Alexa Fluor 596, Invitrogen) diluted at 1:1000 in blocking buffer for 2 hours at room temperature. After three washes with PBS, Prolong Gold with DAPI (Invitrogen) was applied to each section and the slides were covered with glass coverslips. Then, slides were allowed to cure at 4°C before storing at -80°C. Images were acquired with an Olympus IX71 microscope with cellSens software (Olympus, Center Valley, PA).

2.3.8 Quantification of cellular alignment inside ePCL

Immunofluorescence of α-SMA and GFP was used to assess the alignment of cells within the ePCL scaffold. The alignment measurement was carried out with the NIH ImageJ software plug-in named OrientationJ to calculate the directional coherency coefficient [26]. The coherency coefficient ranges from 0 to 1, with 1 indicating a strongly coherent orientation or for this study, greater cellular alignment. To assess the fiber orientation of bare ePCL scaffolds, 3 sample areas were captured. To assess the cell orientation on the surface of the ePCL scaffold under *in vitro* culture, 3 sample areas were captured for both α-SMA and GFP immunostaining. The alignment of cells inside the ePCL scaffold was evaluated at the following four experimental configurations: (1) aligned ePCL scaffold without SMS seeding, 2 weeks *in vivo*. Approximately 100 sample areas of 6 scaffolds from 4 different animals were analyzed. (2) random ePCL scaffold without SMS seeding, 2 weeks *in vivo*. Approximately 140 sample areas of 4 scaffolds from 2 different animals were analyzed. (3) aligned ePCL scaffold with SMS seeding, 3 weeks *in vitro* culture followed by 4 days *in vivo*. Approximately 200 sample areas of 6 scaffolds from 3 different animals were analyzed for α-SMA expression and 43 sample areas of 3 scaffolds from 3 different animals were analyzed for GFP expression. (4) random ePCL with SMS seeding, 3 weeks *in vitro* culture followed by 4 days *in vivo*. Approximately 140 sample areas of 4 scaffolds from 2 different animals were analyzed for α-SMA expression and 55 sample areas of 3 scaffolds from 2 different animals were analyzed for GFP expression. For each condition, sample areas were grouped into the upper or lower layer of the x-z or y-z plane and their coherency were compared (Fig. 1E-H).

2.3.9 Statistical Analysis

Two-tailed unpaired Student's t-test was used to compare the results from the image analysis. A level of significance was set at $p < 0.01$. Data were expressed as the mean ± the standard deviation (SD).

2.4 RESULTS

2.4.1 Two-layer Scaffolds

The intestinal circular and longitudinal smooth muscle layers are orthogonally arranged relative to each other (Fig. 1C,D). To mimic this native histological organization, we employed two layers of ePCL scaffolds with aligned fibers seeded with or without SMS. Scaffolds with randomly oriented fibers seeded with or without SMS were used as comparisons. Two layers of the ePCL scaffolds were assembled from either aligned or randomly oriented fibers by adding collagen gel between two sheets of ePCL. In order to examine the cellular alignment inside the ePCL scaffolds, two-layer scaffolds were cut in orthogonal planes to expose cross sections in x-z and y-z planes (Fig. 1). For the two-layer scaffold with aligned fibers arranged in orthogonal directions, the cross section exposing the x-z plane would cut "perpendicular" to aligned fibers in the upper layer (shown in blue in Fig. 1F) and "parallel" to aligned fibers in the lower layer (shown in green in Fig. 1F). Conversely, the cross section exposing the y-z plane would cut "parallel" to aligned fibers in the upper layer (shown in blue in Fig. 1F) and "perpendicular" to aligned fibers in the lower layer (shown in green in Fig. 1F). In contrast, the ePCL construct with two layers of randomly oriented fibers would appear similar in the x-z and y-z plane cross sections (Fig. 1H).

2.4.2 Scaffold characterization

The difference between ePCL scaffolds with aligned or randomly oriented fibers was examined by SEM (Fig. 2A-D). Aligned ePCL scaffolds had individual fibers 1-5 μm in diameter and most fibers existed individually without crossover (Fig. 2C). Randomly oriented ePCL scaffolds had similar fiber size, with most fibers intertwined with each other (Fig. 2D). Analysis of the fibers showed that the coherency factor of aligned ePCL scaffolds was statistically higher (0.555±0.058 vs. 0.060±0.030; $p = 1.91e\text{-}04 < 0.01$) than that of the randomly oriented ePCL scaffolds (Fig. 2E).

2.4.3 Quantification of in vitro cellular alignment (x-y plane)

Following two weeks of culture *in vitro*, the difference in alignment of cells on the surface of aligned and randomly oriented ePCL scaffolds (x-y plane) was evaluated by the expression of α-SMA (Fig. 2G,H) and GFP (Fig. 2J,K). Analysis of the coherency factor from immunostained images showed that cells cultured on aligned ePCL scaffolds were statistically more aligned (α-SMA: 0.385±0.023 vs. 0.103±0.011; $p = 4.36e\text{-}05 < 0.01$, GFP: 0.309±0.013 vs. 0.079±0.013; $p = 2.75e\text{-}05 < 0.01$) than cells cultured on randomly oriented ePCL scaffolds for both markers (Fig. 2F,I).

2.4.4 Quantification of infiltrating host cells' alignment inside two-layer ePCL scaffolds (x-z and y-z planes)

After two weeks of implantation, the alignment of infiltrating host cells into the two-layer ePCL scaffolds without seeded SMS was analyzed by immnuostaining for α-SMA and by HE (Fig. 3,4). Host cell infiltration inside ePCL scaffolds with two layers of orthogonally aligned fibers

(Fig. 3) mimicked the cellular alignment of intestinal circular and longitudinal smooth muscle layers (Fig. 1C,D). The alignment of upper and lower layers was completely exchanged when the cross section was switched from the x-z to the y-z plane. The upper layer had “perpendicular” and lower layer had “parallel” alignment to the cross sections in x-z plane, while the upper layer had “parallel” and lower layer had “perpendicular” alignment to the cross sections in y-z plane (Fig. 3A-D). In contrast, the upper and lower layers in ePCL scaffolds with randomly oriented fibers demonstrated similar cellular alignment for both cross sections in the x-z and y-z planes (Fig. 4A-D).

Coherency analysis of α-SMA expression for two-layer ePCL scaffolds with aligned fibers confirmed that cells in the lower layer were statistically more aligned (0.402±0.039 vs. 0.191±0.045; $p = 2.22e\text{-}05 < 0.01$) than cells in the upper layer in x-z plane, while cells in the upper layer were statistically more aligned (0.424±0.039 vs. 0.212±0.055; $p = 1.59e\text{-}05 < 0.01$) than cells in the lower layer in y-z plane (Fig. 3E). The coherency distribution in the x-z plane showed that most of the cells in lower layer were more aligned than those in the upper layer with little overlap (Fig. 3F).

In contrast, coherency analysis of α-SMA expression for two-layer ePCL scaffolds with randomly oriented fibers demonstrated no statistical difference in cellular alignment between upper and lower layers in both x-z plane cross sections (0.334±0.056 vs. 0.345±0.055; $p = 0.798 > 0.01$) and y-z plane cross sections (0.355±0.014 vs. 0.313±0.023; $p = 0.020 > 0.01$) (Fig. 4E). The coherency distribution in the x-z plane showed that most of the cells in upper and lower layers had similar cellular alignment, as demonstrated by the extensive overlap (Fig. 4F).

2.4.5 Quantification of cellular alignment inside SMS-seeded two-layer ePCL scaffolds (x-z and y-z planes)

After three weeks of *in vitro* culture followed by 4 days of implantation, cellular alignment inside SMS-seeded two-layer ePCL scaffolds was analyzed by HE staining and immunostaining for α-SMA (Fig. 5,6) and GFP (Fig. 7,8). Since α-SMA and HE stained cells from both seeded SMS and host, GFP was used to examine the cellular alignment from seeded SMS.

Similar to the infiltrating host cells, the alignment of GFP-positive cells in upper and lower layers in aligned ePCL scaffolds was completely reversed when the cross section was switched from the x-z to the y-z plane. The upper layer had "perpendicular" and lower layer had "parallel" alignment to the cross sections in x-z plane, while the upper layer had "parallel" and lower layer had "perpendicular" alignment to the cross sections in y-z plane (Fig. 5A-D, 7A-D). Conversely, GFP-positive cells in the upper and lower layers in ePCL scaffolds with randomly oriented fibers demonstrated similar cellular alignment for both cross sections in the x-z and y-z planes (Fig. 6A-D, 8A-D).

Coherency analysis of α-SMA and GFP expressions for aligned two-layer ePCL scaffolds again demonstrated that cells in the lower layer were statistically more aligned (α-SMA: 0.416±0.032 vs. 0.238±0.040; $p = 6.85e\text{-}06 < 0.01$, GFP: 0.423±0.017 vs. 0.251±0.041; $p = 2.47e\text{-}03 < 0.01$) than cells in the upper layer in x-z plane, while cells in the upper layer were statistically more aligned (α-SMA: 0.458±0.050 vs. 0.178±0.029; $p = 6.85e\text{-}06 < 0.01$, GFP: 0.517±0.047 vs. 0.277±0.028; $p = 1.60e\text{-}03 < 0.01$) than cells in the lower layer in y-z plane (Fig. 5E, 7E). The coherency distribution in x-z plane showed that most of the cells in lower layer were more aligned than those in the upper layer with little overlap (Fig. 5F, 7F).

In contrast, coherency analysis of α-SMA and GFP expressions for random two-layer ePCL scaffolds showed no statistical differences in cellular alignment between upper and lower layers in both x-z plane cross sections (α-SMA: 0.351±0.059 vs. 0.347±0.020; $p = 0.909 > 0.01$, GFP: 0.373±0.033 vs. 0.389±0.008; $p = 0.461 > 0.01$) and y-z plane cross sections (α-SMA: 0.309±0.041 vs. 0.327±0.043; $p = 0.565 > 0.01$, GFP: 0.357±0.038 vs. 0.373±0.046; $p = 0.664 > 0.01$) (Fig. 6E, 8E). The coherency distribution in x-z plane showed that most of the cells in upper and lower layers had similar cellular alignment with extensive overlap (Fig. 6F, 8F).

2.4.6 Summary of cellular alignment inside two-layer ePCL scaffolds (x-z and y-z planes)

For both x-z and y-z planes of two-layer ePCL scaffolds with orthogonally aligned fibers, the highest coherency factor was associated with cross sections that were cut "parallel" to aligned fibers (above 0.4), whereas the coherency factor was significantly lower when cross sections were taken "perpendicular" to aligned fibers (below 0.3). The layers of randomly aligned ePCL scaffolds consistently had average coherency factors that fell between 0.3 and 0.4 (Fig. 3-8E). In addition, the coherency distribution of x-z plane analysis displayed Gaussian distribution (Fig. 3-8F). These results occurred for cells from both host and seeded SMS, thus validating that the fiber alignment of ePCL had influenced the cellular alignment inside two-layer scaffolds (Fig. 3-8).

2.5 DISCUSSION

We demonstrated that orthogonally aligned ePCL scaffolds could induce cellular alignment similar to intestinal circular and longitudinal smooth muscle layers. In contrast, ePCL scaffolds with randomly oriented fibers did not produce such distinguishable cellular alignment. Cells

from both seeded SMS and host infiltrated into the entire depth of the two-layer ePCL scaffolds. These results suggested that cells tended to elongate along the fiber direction not only on the surface of ePCL, but also inside the ePCL after infiltration.

While previous studies have shown 2D cellular alignment with oriented fibers (x-y plane) [2,5–9,22], our study has demonstrated that this approach is also applicable to 3D cellular alignment in vivo (x-z and y-z planes). We chose FDA-approved ePCL as scaffolds for clinically translatable practice. As a result, with only gelatin coating of the ePCL, cells from both seeded SMS and host aligned and elongated along the fiber directions inside the ePCL scaffolds. This system can be useful in tissue regeneration where alignment is essential: vasculature [2,3,27], myocardial tissue [4], musculoskeletal tissue [5], nervous system [6,7], and connective tissue [8,9].

A prior study suggested that the loss of architecture due to rapid degradation of the scaffold prior to the completion of tissue remodeling could impair cellular alignment and cause scar formation [28]. However, ePCL *in vivo* degradation studies showed only 20-30% molecular weight reduction after 3-6 months, without structural deterioration [28–31]. Similarly, in our study, there was no significant degradation of the scaffold at explantation, and ePCL fibers could still been seen on histology. Whether the observed cellular alignment will persist after ePCL degradation is unclear. The cells may still maintain their orientation because the extracellular matrix that replaced the ePCL fibers may also be aligned [32]. Future studies are needed to evaluate the longevity of cellular alignment after degradation of the ePCL.

Our ultimate goal is to construct fully functional intestinal smooth muscle layers capable of peristalsis. Future studies will use this system as a foundation to mimic the intestinal smooth muscle layers, by adding additional components into the two orthogonally aligned ePCL

scaffolds. For example, purified enteric neuronal cells and interstitial cells of Cajal can be seeded in-between the two-layer ePCL scaffolds to serve as the myenteric plexus and aid intestinal smooth muscle cells by providing the necessary signals for peristalsis. Intestinal constructs fabricated from this two-layer aligned ePCL may be used to generate full-thickness intestine useful for the treatment of short bowel syndrome or inflammatory bowel disease [33–36].

2.6 CONCLUSION

Our study demonstrated that orthogonally aligned ePCL scaffolds can regenerate the cellular alignment of native intestinal circular and longitudinal smooth muscle layers. Our analysis quantitatively confirmed that cells align along the ePCL fibers not only on the surface (x-y plane) but also inside of the ePCL scaffolds (x-z & y-z planes). Future development of this system by adding myenteric plexus components will promote the creation of more functional intestinal smooth muscle layers. Similarly, this system can be applied to other types of tissues engineering that require alignment. Our investigation validated the significance of fiber alignment within scaffolds for engineering three dimensionally aligned tissues.

2.7 ACKNOWLEDGEMENTS

We thank UCLA Translational Pathology Core Lab for histologic processing. This work was funded by an R01 DK083119 from the National Institutes of Health.

2.8 FIGURES

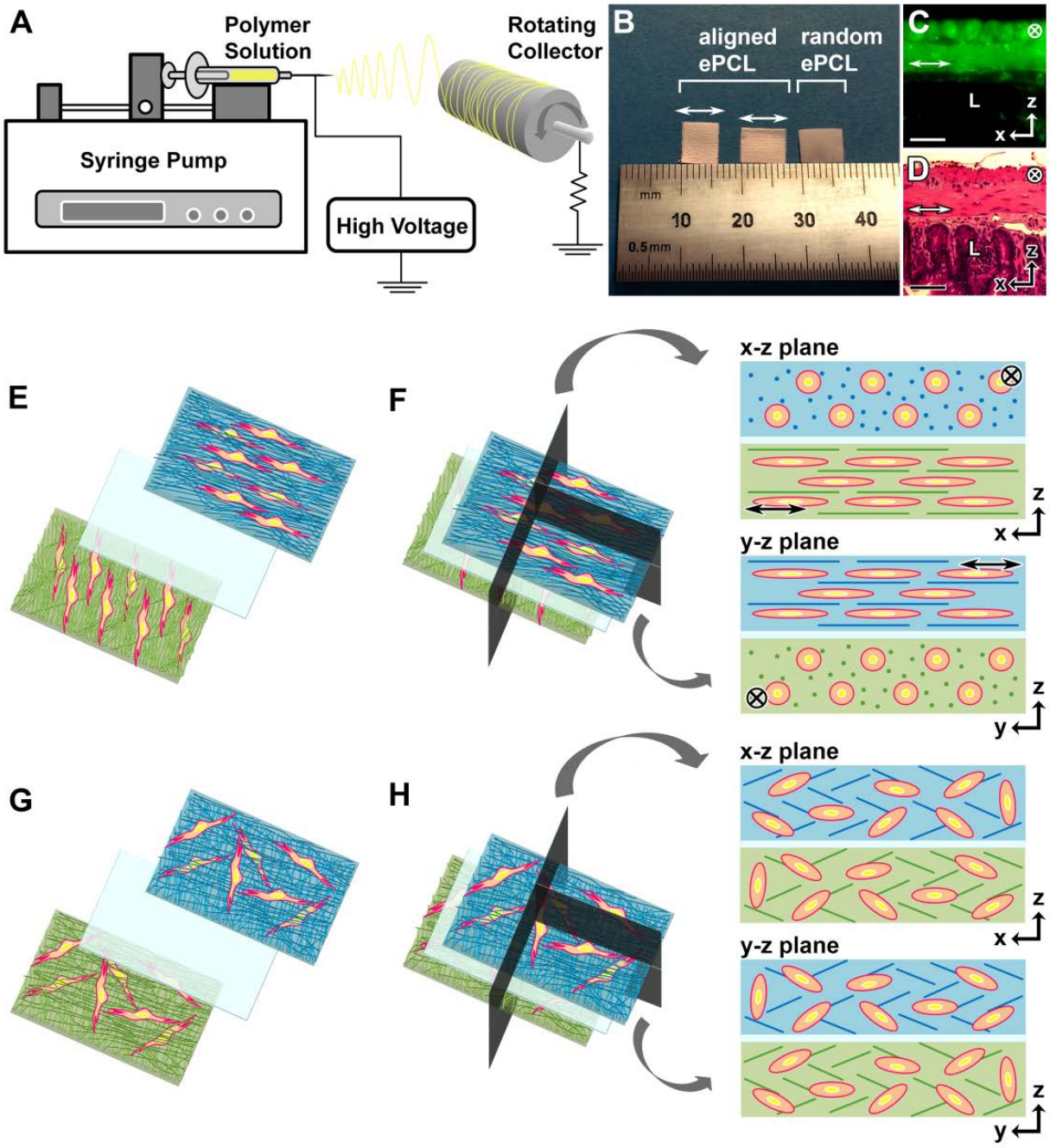

Fig. 1. Schematic diagram of two-layer scaffolds for mimicking small intestine layers. (A) Basic setup for fabricating electrospun polypolycaprolactone (ePCL) sheets. (B) Laser cut ePCL scaffolds with aligned and random fibers. (C) Immunofluorescence of smooth muscle actin (α-SMA) expression and (D) HE

staining of adult, mouse small intestine in cross section. Preparation of two-layer ePCL scaffolds with (E) aligned or (G) randomly oriented fibers for implantation. In order to mimic the intestinal circular and longitudinal muscle layers, two-layer ePCL scaffolds with orthogonally oriented fibers were seeded with intestinal smooth muscles strips (SMS) and connected with a thin collagen gel before implantation. Two-layer ePCL scaffolds with randomly oriented fibers were used as controls. To compare the cell alignment inside the ePCL, two-layer scaffolds with (F) aligned or (H) randomly oriented fibers were cut in two perpendicular planes to expose cross sections in x-z and y-z planes. Scale bar = 50 μm. L = Lumen. ⊗ = alignment perpendicular to the cross section. ↔ = alignment parallel to the cross section.

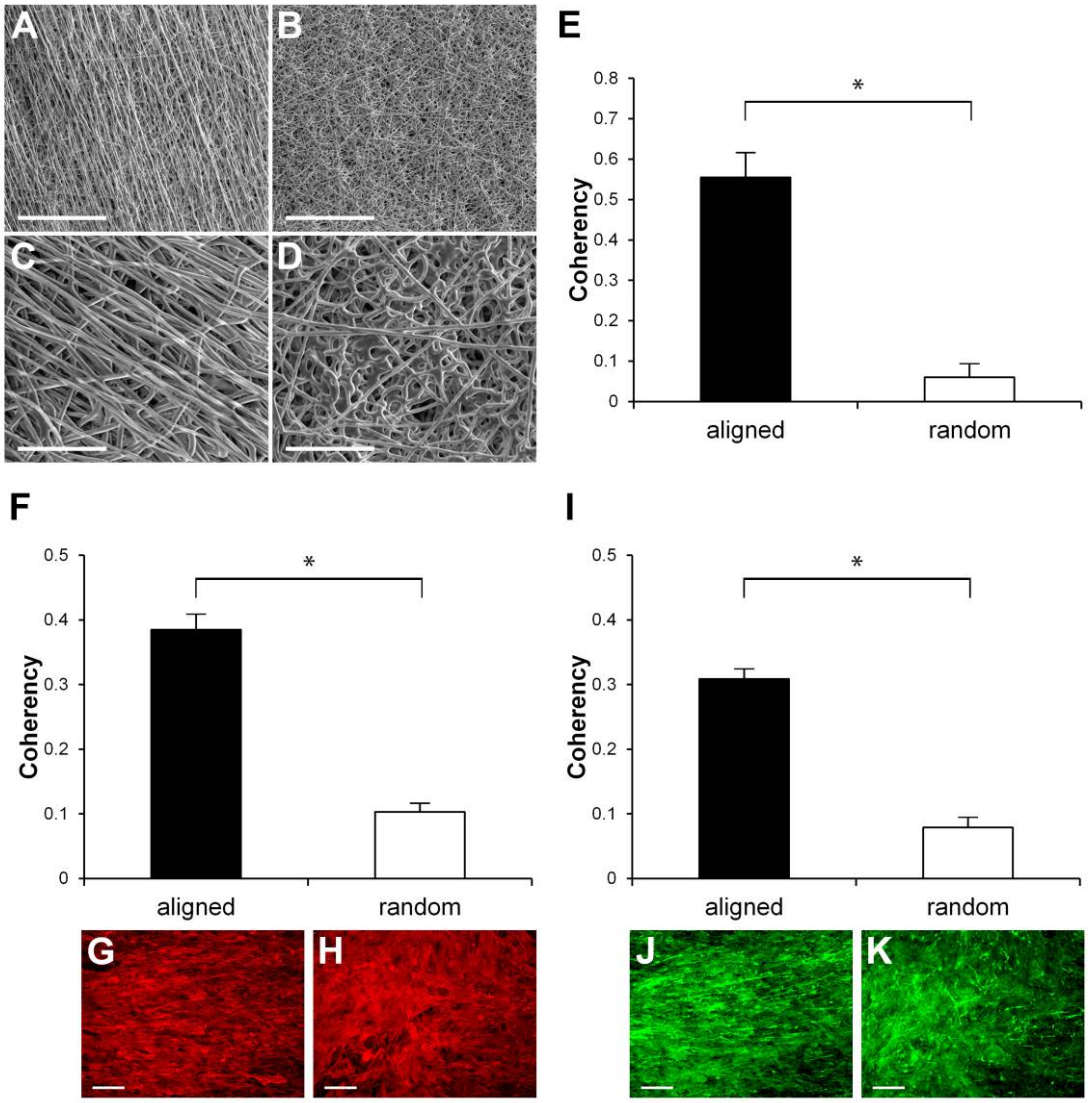

Fig. 2. Alignment of cells on SMS-seeded ePCL scaffolds. Scanning electron micrographs of ePCL with (A, C) aligned and (B, D) randomly oriented fibers at 250x and 1000x magnifications. (E) Coherency analysis of aligned and random ePCL (n=3). Scaffolds were seeded with SMS and immunostained at day 14. Images were taken to show the cell alignment on the ePCL surface (x-y plane). (G, H) α-SMA and (J, K) green fluorescent protein (GFP) expression of SMS seeded on (G, J) aligned and (H, K) random ePCL. Coherency analysis of (F) α-SMA (n=3) and (I) GFP (n=3) expression of SMS seeded on aligned and random ePCL. *$p < 0.01$. Error bar = SD. Scale bar A, B, G, H, J, K = 200 µm; scale bar C, D = 50 µm.

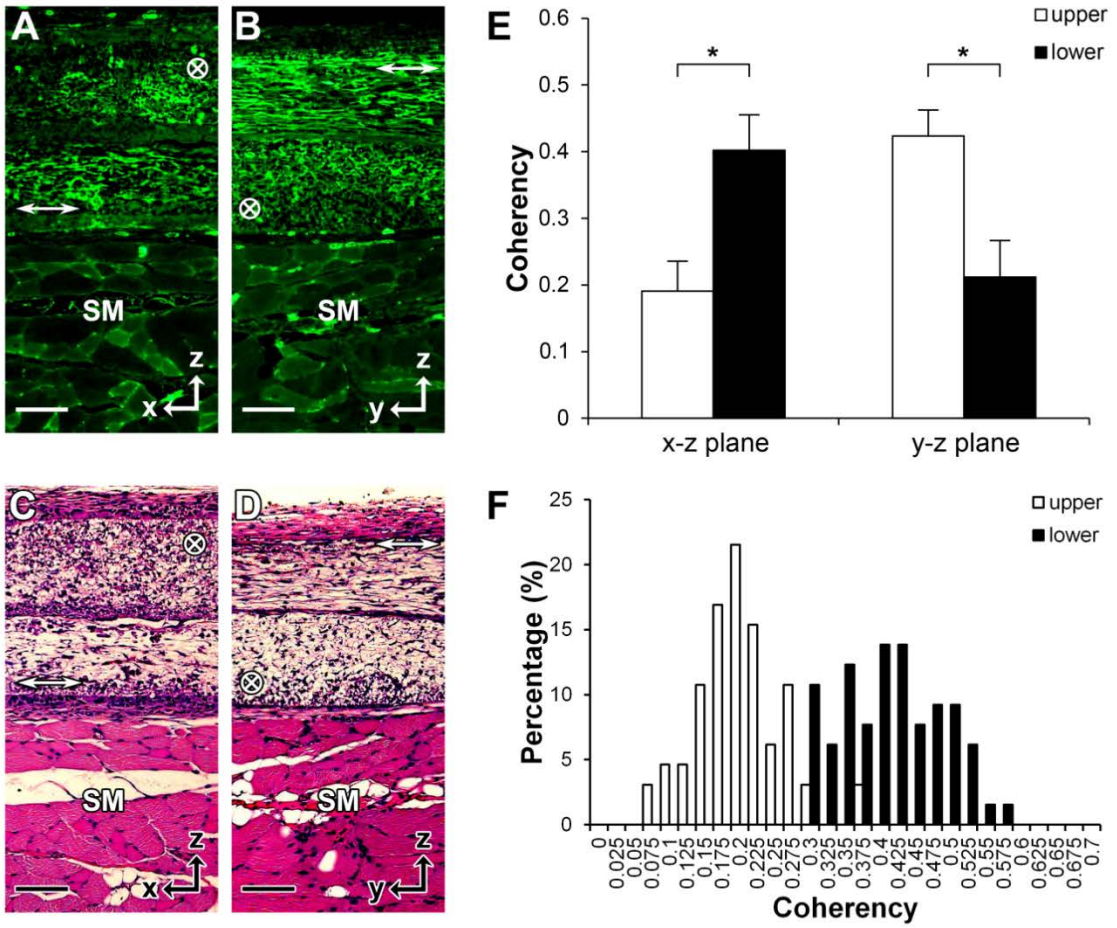

Fig. 3. Quantification of α-SMA alignment expressed by infiltrating host cells inside two-layer ePCL scaffolds with aligned fibers. ePCL scaffolds were retrieved on day 14 after implantation. α-SMA expression of infiltrating host cells inside aligned ePCL scaffolds in the (A) x-z and (B) y-z planes. HE staining of infiltrating host cells inside aligned ePCL scaffolds on the (C) x-z and (D) y-z planes. (E) Coherency analysis and (F) the distribution (x-z plane as representative) of α-SMA alignment of infiltrating host cells inside two-layer aligned ePCL scaffolds (n=6). *p < 0.01. Error bar = SD. Scale bar = 100 μm. SM = Skeletal Muscle. ⊗ = alignment perpendicular to the cross section. ↔ = alignment parallel to the cross section.

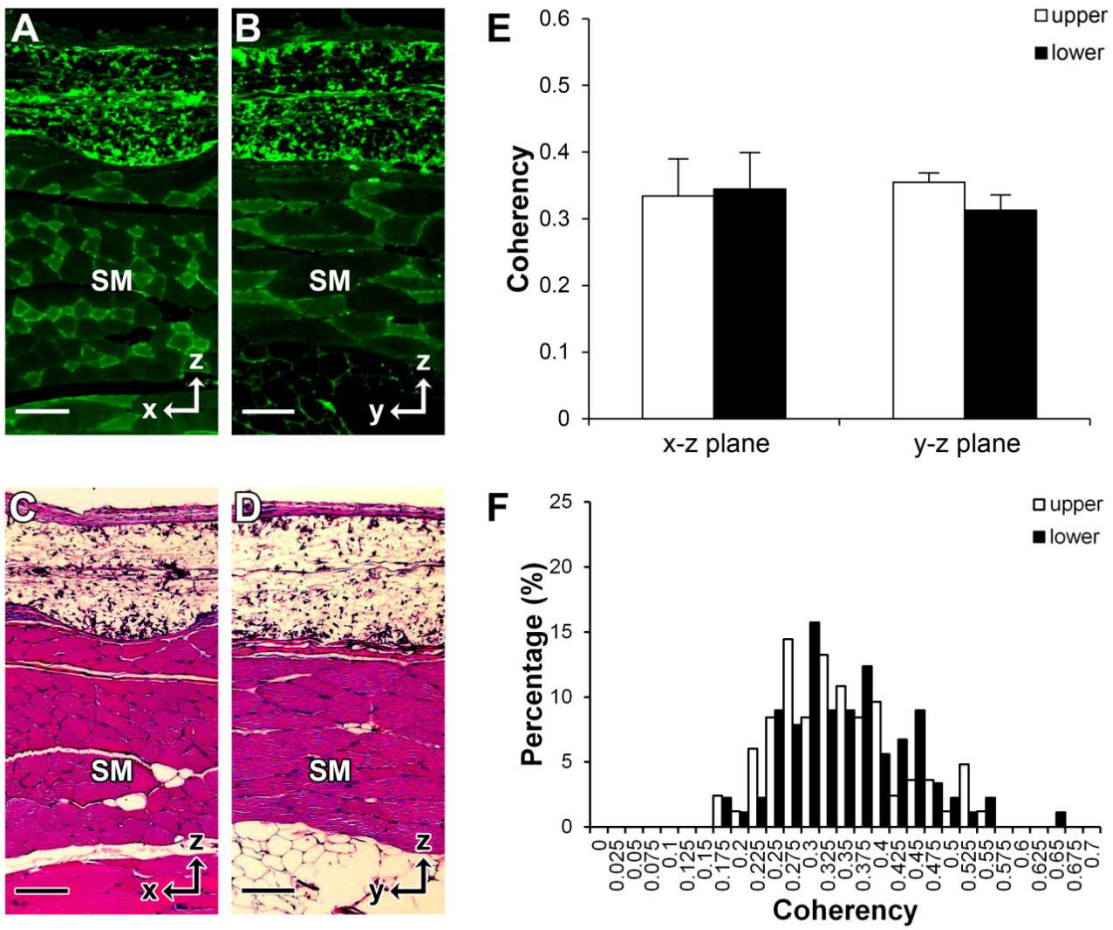

Fig. 4. Quantification of α-SMA alignment of infiltrating host cells inside two-layer ePCL scaffolds with randomly oriented fibers. ePCL scaffolds were retrieved on day 14 after implantation. α-SMA expression of infiltrating host cells inside randomly oriented ePCL scaffolds on the (A) x-z and (B) y-z planes. HE staining of infiltrating host cells inside randomly oriented ePCL scaffolds on the (C) x-z and (D) y-z planes. (E) Coherency analysis and (F) the distribution (x-z plane as representative) of α-SMA alignment of infiltrating host cells inside two-layer random ePCL scaffolds (n=4). $p > 0.01$. Error bar = SD. Scale bar = 100 μm. SM = Skeletal Muscle.

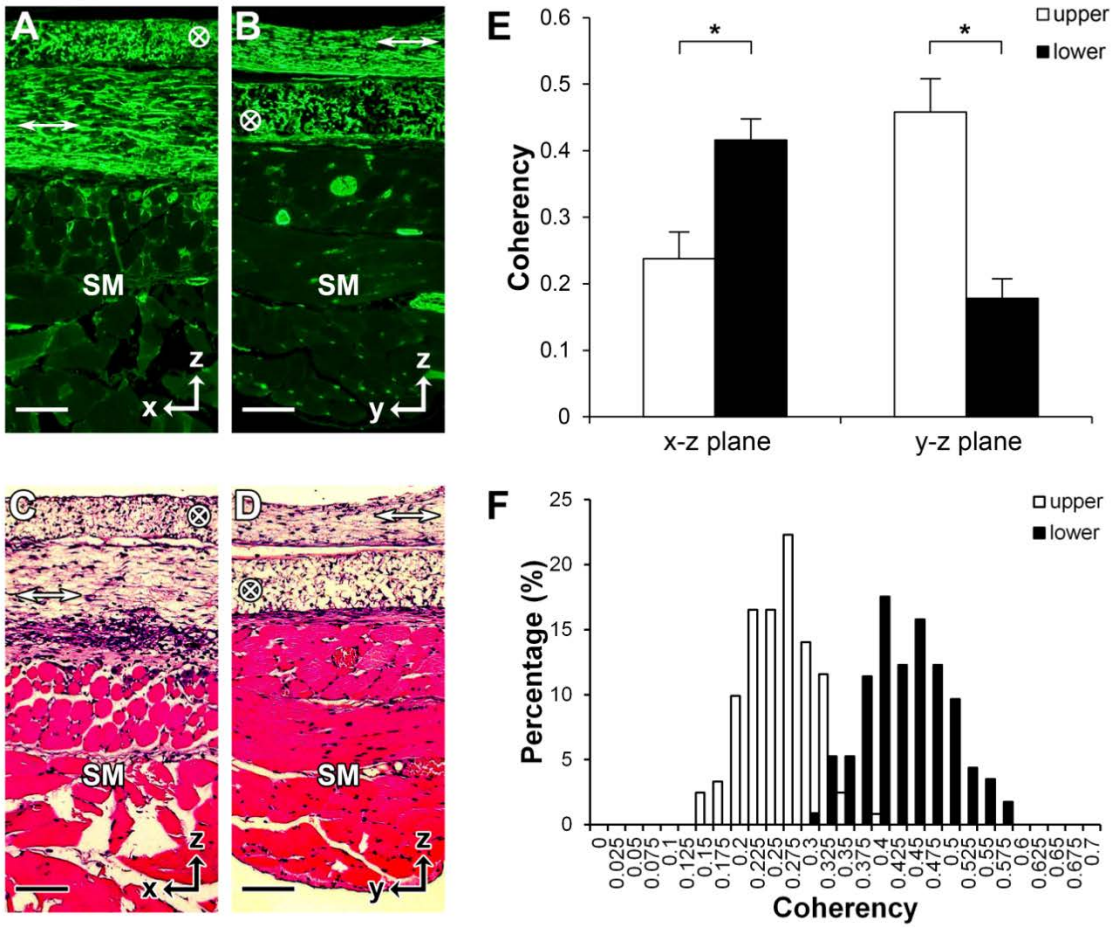

Fig. 5. Quantification of α-SMA alignment of seeded SMS and infiltrating host cells inside two-layer ePCL scaffolds with aligned fibers. ePCL scaffolds were cultured *in vitro* for 3 weeks and retrieved on day 4 after implantation. α-SMA expression of seeded SMS and infiltrating host cells inside aligned ePCL scaffolds on the (A) x-z and (B) y-z planes. HE staining of seeded SMS and infiltrating host cells inside aligned ePCL scaffolds on the (C) x-z and (D) y-z planes. (E) Coherency analysis and (F) the distribution (x-z plane as representative) of α-SMA alignment of seeded SMS and infiltrating host cells inside two-layer aligned ePCL scaffolds (n=6). *$p < 0.01$. Error bar = SD. Scale bar = 100 μm. SM = Skeletal Muscle. ⊗ = alignment perpendicular to the cross section. ↔ = alignment parallel to the cross section.

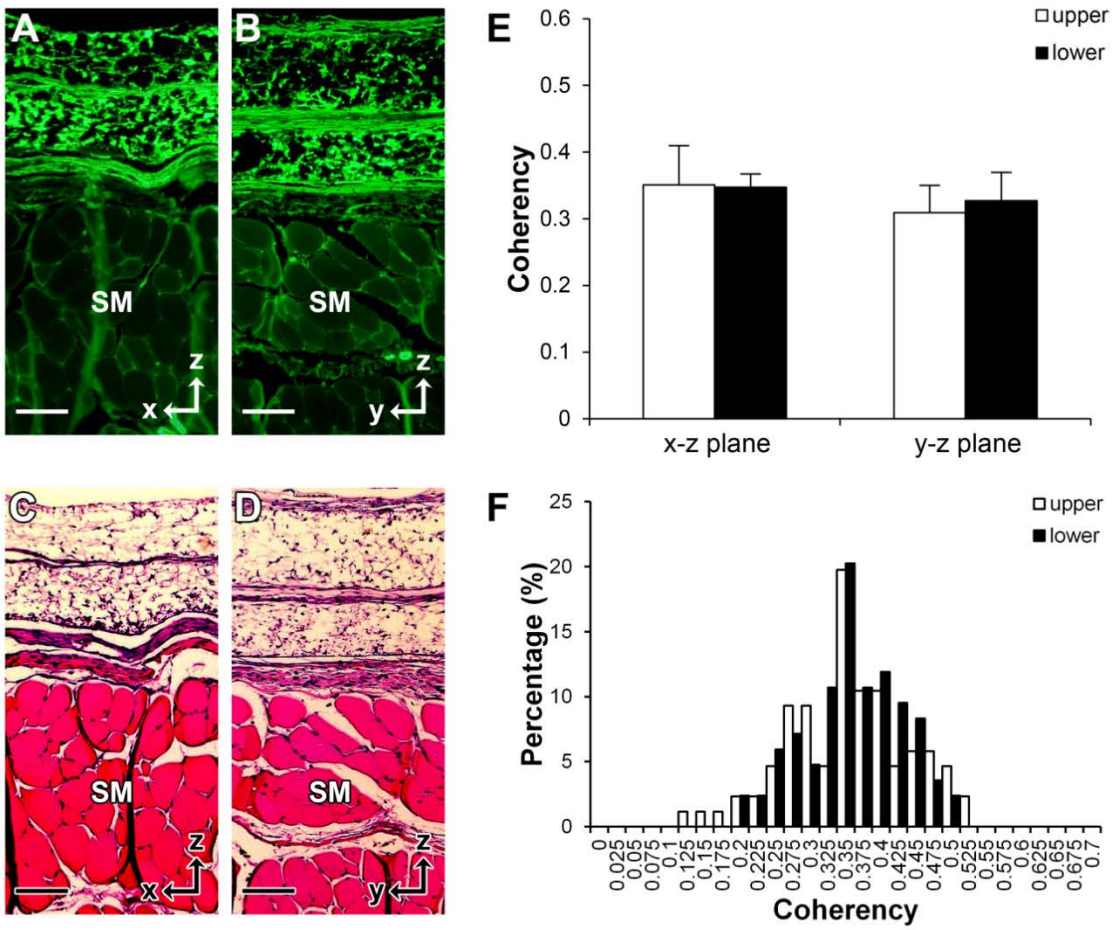

Fig. 6. Quantification of α-SMA alignment of seeded SMS and infiltrating host cells inside two-layer ePCL scaffolds with randomly oriented fibers. ePCL scaffolds were cultured *in vitro* for 3 weeks and retrieved on day 4 after implantation. α-SMA expression of seeded SMS and infiltrating host cells inside randomly oriented ePCL scaffolds on the (A) x-z and (B) y-z planes. HE staining of seeded SMS and infiltrating host cells inside randomly oriented ePCL scaffolds on the (C) x-z and (D) y-z planes. (E) Coherency analysis and (F) the distribution (x-z plane as representative) of α-SMA alignment of seeded SMS and infiltrating host cells inside two-layer random ePCL scaffolds (n=4). $p > 0.01$. Error bar = SD. Scale bar = 100 μm. SM = Skeletal Muscle.

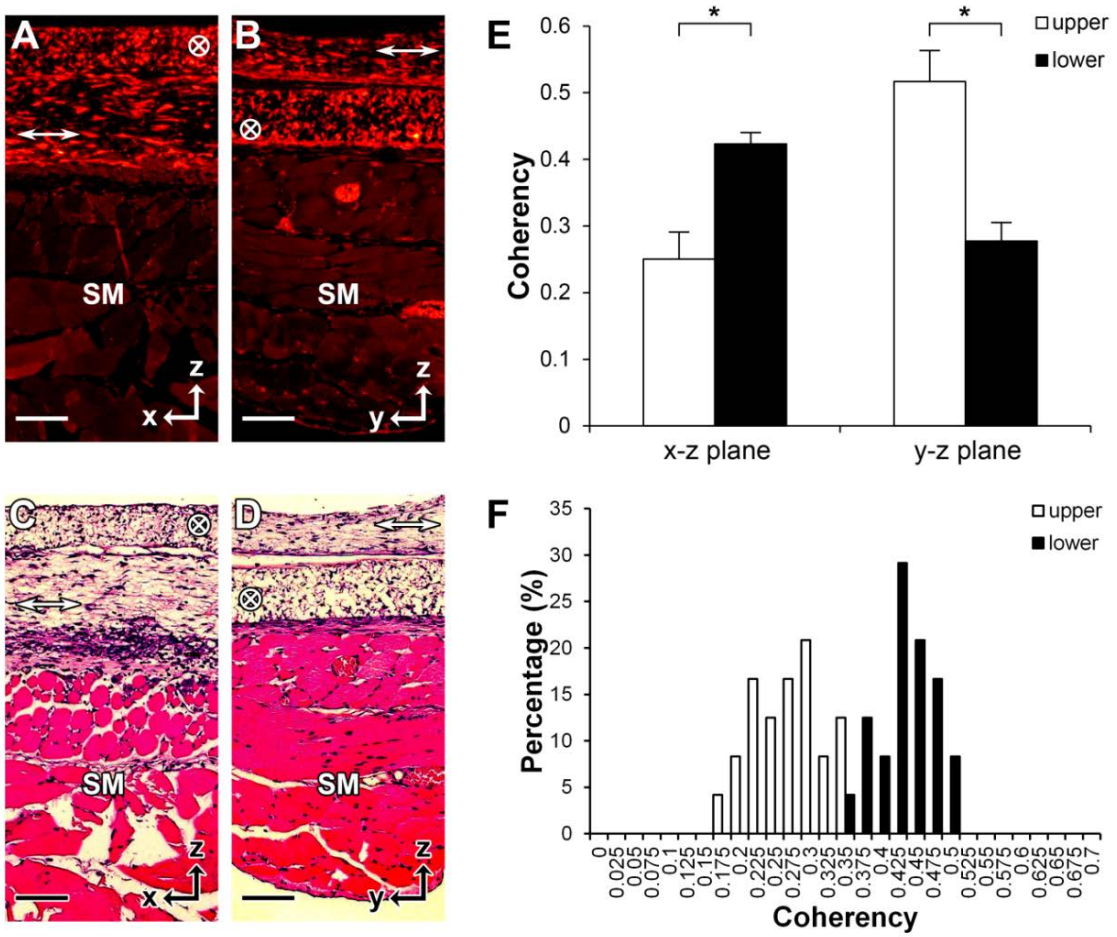

Fig. 7. Quantification of GFP alignment of seeded SMS inside two-layer ePCL scaffolds with aligned fibers. ePCL scaffolds were cultured *in vitro* for 3 weeks and retrieved on day 4 after implantation. GFP expression of seeded SMS inside aligned ePCL scaffolds on the (A) x-z and (B) y-z planes. HE staining of seeded SMS inside aligned ePCL scaffolds on the (C) x-z and (D) y-z planes. (E) Coherency analysis and (F) the distribution (x-z plane as representative) of GFP alignment of seeded SMS inside two-layer aligned ePCL scaffolds (n=3). *p < 0.01. Error bar = SD. Scale bar = 100 μm. SM = Skeletal Muscle. Note: Fig. 5 and Fig. 7 are the same locations. ⊗ = alignment perpendicular to the cross section. ↔ = alignment parallel to the cross section.

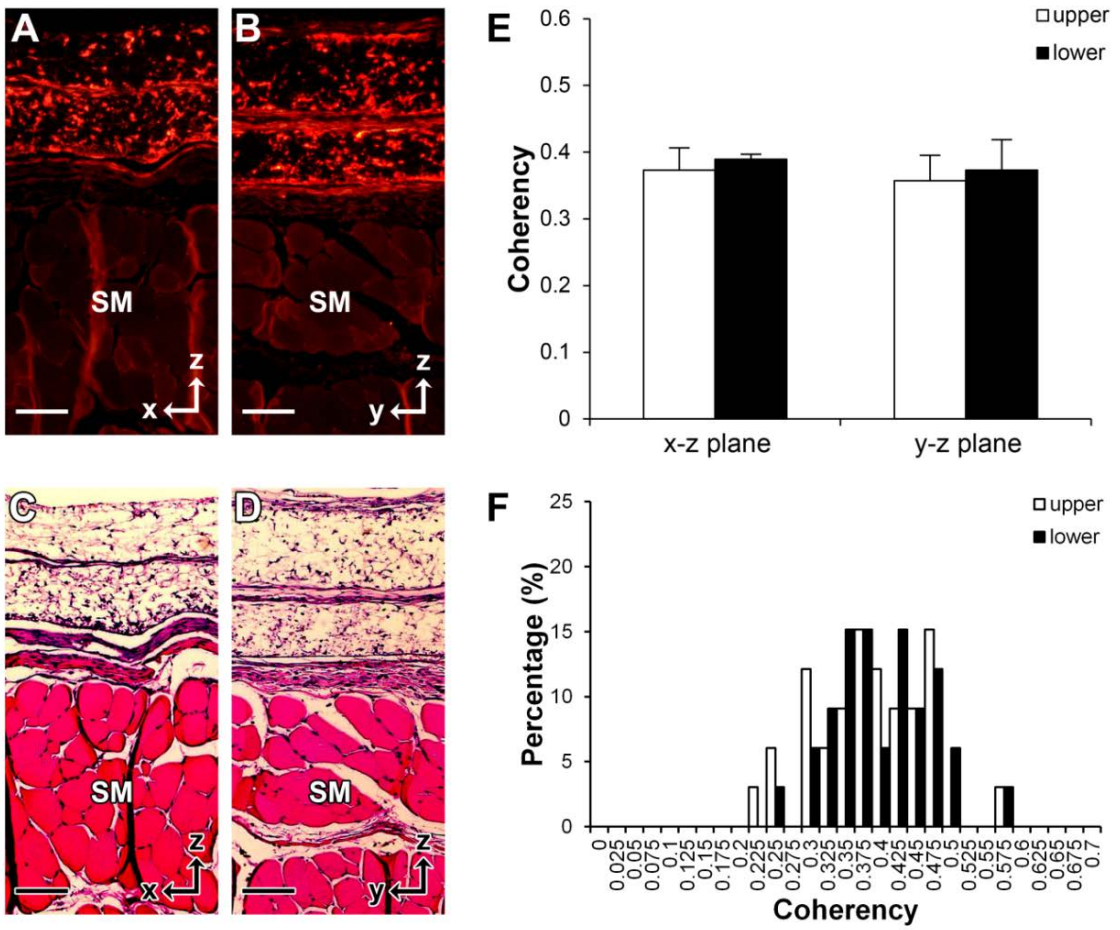

Fig. 8. Quantification of GFP alignment of seeded SMS inside two-layer ePCL scaffolds with randomly oriented fibers. ePCL scaffolds were cultured *in vitro* for 3 weeks and retrieved on day 4 after implantation. GFP expression of seeded SMS inside randomly oriented ePCL scaffolds on the (A) x-z and (B) y-z planes. HE staining of seeded SMS inside randomly oriented ePCL scaffolds on the (C) x-z and (D) y-z planes. (E) Coherency analysis and (F) the distribution (x-z plane as representative) of GFP alignment of seeded SMS inside two-layer random ePCL scaffolds (n=3). $p > 0.01$. Error bar = SD. Scale bar = 100 μm. SM = Skeletal Muscle. Note: Fig. 6 and Fig. 8 are the same locations.

2.9 REFERENCES

[1] Bitar KN, Raghavan S, Zakhem E. Tissue engineering in the gut: developments in neuromusculature. Gastroenterology 2014;146:1614–24. doi:10.1053/j.gastro.2014.03.044.

[2] Chiu J-J, Chen L-J, Chen C-N, Lee P-L, Lee C-I. A model for studying the effect of shear stress on interactions between vascular endothelial cells and smooth muscle cells. J Biomech 2004;37:531–9. doi:10.1016/j.jbiomech.2003.08.012.

[3] Nerem RM, Seliktar D. Vascular tissue engineering. Annu Rev Biomed Eng 2001;3:225–43. doi:10.1146/annurev.bioeng.3.1.225.

[4] Papadaki M, Bursac N, Langer R, Merok J, Vunjak-Novakovic G, Freed LE. Tissue engineering of functional cardiac muscle: molecular, structural, and electrophysiological studies. Am J Physiol Hear Circ Physiol 2001;280:H168-178.

[5] Li W-J, Mauck RL, Cooper J a, Yuan X, Tuan RS. Engineering controllable anisotropy in electrospun biodegradable nanofibrous scaffolds for musculoskeletal tissue engineering. J Biomech 2007;40:1686–93. doi:10.1016/j.jbiomech.2006.09.004.

[6] Yang F, Murugan R, Wang S, Ramakrishna S. Electrospinning of nano/micro scale poly(L-lactic acid) aligned fibers and their potential in neural tissue engineering. Biomaterials 2005;26:2603–10. doi:10.1016/j.biomaterials.2004.06.051.

[7] Kim Y-T, Haftel VK, Kumar S, Bellamkonda R V. The role of aligned polymer fiber-based constructs in the bridging of long peripheral nerve gaps. Biomaterials 2008;29:3117–27. doi:10.1016/j.biomaterials.2008.03.042.

[8] Liu Y, Ramanath HS, Wang D-A. Tendon tissue engineering using scaffold enhancing strategies. Trends Biotechnol 2008;26:201–9. doi:10.1016/j.tibtech.2008.01.003.

[9] Vunjak-Novakovic G, Altman G, Horan R, Kaplan DL. Tissue engineering of ligaments. Annu Rev Biomed Eng 2004;6:131–56. doi:10.1146/annurev.bioeng.6.040803.140037.

[10] Ionescu LC, Mauck RL. Porosity and Cell Preseeding Influence Electrospun Scaffold Maturation and Meniscus Integration In Vitro. Tissue Eng Part A 2013;19:538–47. doi:10.1089/ten.tea.2012.0052.

[11] Ayres C, Bowlin GL, Henderson SC, Taylor L, Shultz J, Alexander J, et al. Modulation of anisotropy in electrospun tissue-engineering scaffolds: Analysis of fiber alignment by the fast Fourier transform. Biomaterials 2006;27:5524–34. doi:10.1016/j.biomaterials.2006.06.014.

[12] Courtney T, Sacks MS, Stankus J, Guan J, Wagner WR. Design and analysis of tissue engineering scaffolds that mimic soft tissue mechanical anisotropy. Biomaterials 2006;27:3631–8. doi:10.1016/j.biomaterials.2006.02.024.

[13] Reneker DH, Chun I. Nanometre diameter fibres of polymer, produced by electrospinning. Nanotechnology 1996;7:216–23. doi:10.1088/0957-4484/7/3/009.

[14] Li M, Mondrinos MJ, Gandhi MR, Ko FK, Weiss AS, Lelkes PI. Electrospun protein fibers as matrices for tissue engineering. Biomaterials 2005;26:5999–6008. doi:10.1016/j.biomaterials.2005.03.030.

[15] Xu C, Yang F, Wang S, Ramakrishna S. In vitro study of human vascular endothelial cell function on materials with various surface roughness. J Biomed Mater Res A 2004;71:154–61. doi:10.1002/jbm.a.30143.

[16] Li W-J, Jiang YJ, Tuan RS. Chondrocyte phenotype in engineered fibrous matrix is regulated by fiber size. Tissue Eng 2006;12:1775–85. doi:10.1089/ten.2006.12.1775.

[17] Lee CH, Shin HJ, Cho IH, Kang Y-M, Kim IA, Park K-D, et al. Nanofiber alignment and direction of mechanical strain affect the ECM production of human ACL fibroblast. Biomaterials 2005;26:1261–70. doi:10.1016/j.biomaterials.2004.04.037.

[18] Nerurkar NL, Elliott DM, Mauck RL. Mechanics of Oriented Electrospun Nanofibrous Scaffolds for Annulus Fibrosus Tissue Engineering 2007:1018–28. doi:10.1002/jor.

[19] Ayres CE, Bowlin GL, Pizinger R, Taylor LT, Keen C a, Simpson DG. Incremental changes in anisotropy induce incremental changes in the material properties of electrospun scaffolds. Acta Biomater 2007;3:651–61. doi:10.1016/j.actbio.2007.02.010.

[20] Li W-J, Cooper J a, Mauck RL, Tuan RS. Fabrication and characterization of six electrospun poly(alpha-hydroxy ester)-based fibrous scaffolds for tissue engineering applications. Acta Biomater 2006;2:377–85. doi:10.1016/j.actbio.2006.02.005.

[21] Baker BM, Mauck RL. The effect of nanofiber alignment on the maturation of engineered meniscus constructs. Biomaterials 2007;28:1967–77. doi:10.1016/j.biomaterials.2007.01.004.

[22] Baker BM, Gee AO, Metter RB, Nathan AS, Marklein RA, Burdick JA, et al. The potential to improve cell infiltration in composite fiber-aligned electrospun scaffolds by the selective removal of sacrificial fibers. Biomaterials 2008;29:2348–58.

[23] Geisbauer CL, Chapin JC, Wu BM, Dunn JCY. Transplantation of Enteric Cells Expressing p75 in the Rodent Stomach. J Surg Res 2012;174:257–65. doi:10.1016/j.jss.2010.12.016.

[24] Ordög T, Redelman D, Horowitz NN, Sanders KM. Immunomagnetic enrichment of interstitial cells of Cajal. Am J Physiol Gastrointest Liver Physiol 2004;286:G351-60. doi:10.1152/ajpgi.00281.2003.

[25] Walthers CM, Lee M, Wu BM, Dunn JCY. Smooth muscle strips for intestinal tissue engineering. PLoS One 2014;9:e114850. doi:10.1371/journal.pone.0114850.

[26] Fonck E, Feigl GG, Fasel J, Sage D, Unser M, Rüfenacht D a, et al. Effect of aging on elastin functionality in human cerebral arteries. Stroke 2009;40:2552–6. doi:10.1161/STROKEAHA.108.528091.

[27] Xu C. Aligned biodegradable nanofibrous structure: a potential scaffold for blood vessel engineering. Biomaterials 2004;25:877–86. doi:10.1016/S0142-9612(03)00593-3.

[28] Lorden ER, Miller KJ, Bashirov L, Ibrahim MM, Hammett E, Jung Y, et al. Mitigation of hypertrophic scar contraction via an elastomeric biodegradable scaffold. Biomaterials 2015;43:61–70. doi:10.1016/j.biomaterials.2014.12.003.

[29] Bölgen N, Menceloğlu YZ, Acatay K, Vargel İ, Pişkin E. In vitro and in vivo degradation of non-woven materials made of poly(ε-caprolactone) nanofibers prepared by electrospinning under different conditions. J Biomater Sci Polym Ed 2005;16:1537–55. doi:10.1163/156856205774576655.

[30] Pektok E, Nottelet B, Tille J-C, Gurny R, Kalangos A, Moeller M, et al. Degradation and Healing Characteristics of Small-Diameter Poly(-Caprolactone) Vascular Grafts in the Rat Systemic Arterial Circulation. Circulation 2008;118:2563–70. doi:10.1161/CIRCULATIONAHA.108.795732.

[31] Tillman BW, Yazdani SK, Lee SJ, Geary RL, Atala A, Yoo JJ. The in vivo stability of electrospun polycaprolactone-collagen scaffolds in vascular reconstruction. Biomaterials 2009;30:583–8. doi:10.1016/j.biomaterials.2008.10.006.

[32] Petrigliano FA, Arom GA, Nazemi AN, Yeranosian MG, Wu BM, McAllister DR. In Vivo Evaluation of Electrospun Polycaprolactone Graft for Anterior Cruciate Ligament Engineering. Tissue Eng Part A 2014:150127064142004. doi:10.1089/ten.tea.2013.0482.

[33] Hanauer SB. Inflammatory bowel disease: Epidemiology, pathogenesis, and therapeutic opportunities. Inflamm Bowel Dis 2006;12:S3–9. doi:10.1097/01.MIB.0000195385.19268.68.

[34] Abraham C, Cho JH. Inflammatory bowel disease. N Engl J Med 2009;361:2066–78. doi:10.1056/NEJMra0804647.

[35] Kim ER, Chang DK. Colorectal cancer in inflammatory bowel disease: The risk, pathogenesis, prevention and diagnosis. World J Gastroenterol 2014;20:9872–81. doi:10.3748/wjg.v20.i29.9872.

[36] Coviello LC, Stein SL. Surgical management of nonpolypoid colorectal lesions and strictures in colonic inflammatory bowel disease. Gastrointest Endosc Clin N Am 2014;24:447–54. doi:10.1016/j.giec.2014.04.002.

CHAPTER THREE: INTERSTITIAL CELLS OF CAJAL ENABLE ENGINEERING OF RHYTHMICALLY CONTRACTING INTESTINAL SMOOTH MUSCLE

3.1 ABSTRACT

Oriented smooth muscle layers in the intestine contract rhythmically due to the action of interstitial cells of Cajal (ICC) that serve as pacemakers of the intestine. Disruption of ICC networks has been reported in various intestinal motility disorders, which limit the quality and expectancy of life. A significant challenge in intestinal smooth muscle engineering is the rapid loss of function in cultured ICC and smooth muscle cells (SMC). Here we demonstrate a novel approach to maintain the function of both ICC and SMC *in vitro*. Primary intestinal SMC mixtures cultured on feeder cells seeded electrospun poly(3-caprolactone) scaffolds exhibited rhythmic contractions with directionality for over 10 weeks *in vitro*. The simplicity of this system allows its wide usage in discovery research for motility disorders and tissue engineering.

3.2 INTRODUCTION

The intestine is responsible for digestion, nutrient and water absorption, and waste removal. An increasing number of people are suffering from various intestinal disorders which severely affect their life expectancy and quality of life[1]. According to the Crohn's and Colitis Foundation of America, there are approximately 1.6 million Americans suffering from inflammatory bowel disease in 2014, which is a 0.2 million increase from 2008.

When the intestine fails to function, current medical treatment options have significant limitations: total parenteral nutrition leads to unacceptably high morbidity and mortality rates and transplantation faces donor scarcity, organ rejection, and life-long immunosuppression[2]. Therefore, engineering functional intestinal tissue raises hope as an alternative therapeutic

strategy for patients with intestinal failure. Previous studies have been done to regenerate the intestinal epithelium[3] and many types of muscle, including vascular smooth muscle[5,6], cardiac[7–10] and skeletal muscle[5,11]. However, few have investigated the regeneration of intestinal smooth muscle[12,13].

The aligned smooth muscle layers of the intestine move autonomously. Spontaneous electrical slow waves derived from pacemaker activity of the intestine arrange contractile patterns into phasic contractions that are the basis for peristalsis. Neural or hormonal inputs do not generate the intrinsic pacemaker activity of smooth muscles but affect the degree of coupling between pacemaker activity and contractions[14]. Interstitial cells of Cajal (ICC) are a specialized group of cells responsible for the pacemaker activity in visceral smooth muscles, generating and actively propagating the slow waves[15,16].

Isolated intestinal SMCs may generate fast Ca^{2+} action potentials, but not the spontaneous slow waves in smooth muscles. Conversely, isolated ICC generate spontaneous electrical rhythmicity similar to the electrical activity in intact smooth muscles[17,18]. The binding of stem cell factor (SCF) to the receptor tyrosine kinase Kit induces a signaling pathway in ICC, which is critical for the normal development of ICC and rhythmic activity[19–23]. SCF stimulation of Kit is essential for ICC maintenance [22,24], and Ca^{2+} activated Cl^- channels (Ano1) expressed on ICC were identified as the key conductance responsible for the pacemaker activity[18]. However, ICC comprise less than 10% of the cells within intestinal smooth muscle, and isolated ICC are difficult to maintain in cell culture. ICC tend to lose their characteristic morphologies and Kit immunoreactivity after enzymatic digestion during the cell isolation procedure. Although ICC can grow and develop networks that produce electrical rhythmicity in cell culture, those

dispersed ICC undergo extensive phenotypic changes within a few days, including the apparent loss of the ion channels responsible for the slow wave activity[14,18,25,26].

Using a feeder cell system, we demonstrate a novel protocol where both purified ICC and isolated intestinal smooth muscle cell (ISMC) mixtures can be cultured for weeks *in vitro* with intact pacemaker ability and rhythmic contractions. Disruption of ICC networks and the loss of SMC maturity in intestinal muscularis have been reported in a variety of diseases resulting in intestinal motility disorders leading to pseudo-obstruction, Hirschsprung's disease, inflammatory bowel diseases, and slow transit constipation[27–30]. Therefore, this system provides not only crucial progress in intestinal smooth muscle engineering, but also an *in vitro* platform to investigate cellular phenotypes and mechanisms associated with different intestinal disorders, to screen drugs that may alter motility, and to identify the biomarkers for early diagnosis and clinical stratification.

3.3 RESULTS

3.3.1 ICC proliferation *in vitro*

To enrich the ICC population in culture, immunomagnetic sorting was performed on primary intestinal smooth muscle cell mixture (ISMC Mix, derived from C57BL/6 mouse) that were first cultured on gelatin for 3 days. The resultant MACS+ cells (MACS purified ICC population using antibody to Kit) proliferated on mitomycin-treated STO cells that expressed stem cell factor (SCF). The MACS+ cells exhibited ICC morphology and expressed Kit and Ano1 for up to two weeks in culture (**Fig. 1a-b**). When a 60k per well cell seeding density was used, MACS+ cells spread on STO cells in 48-well plates and became confluent in one week. A lower seeding

density was tested to achieve more cell expansion. MACS+ cells with seeding density of 15k proliferated on STO cells and formed a confluent layer in two week (**Fig. 1a-b**).

STO cells are embryonic fibroblasts commonly used for embryonic stem cell culture. Embryonic fibroblasts derived from the same mouse strain as ISMC Mix (C57BL/6), MEF, were also tested with MACS+ cell culture, with gelatin-coated wells serving as controls. STO cells supported MACS+ cell growth better than gelatin coating and MEF cells (**Fig. 1c-e)**. Although MACS+ cells proliferated on all three conditions (**Fig. 1d**), cells maintained the ICC marker Kit significantly better on STO cells than on MEF or gelatin (**Fig. 1c, 1e** and **Supplementary Fig. 1**). Although with the same 100k cell seeding density, more STO cells than MEF were attached because the size of STO cells is smaller than MEF (**Supplementary Fig. 2a, c**). STO cells expressed significantly higher *kitl* mRNA level at day 0 and after 7 days in culture, and STO cells expressed more SCF protein at day 7 than MEF cells. The difference in SCF expression may be responsible for the difference in ICC survival (**Supplementary Fig. 2b, d, e**). This is further supported by varying STO cell density, which demonstrated a density-dependent proliferation of MACS+ cells[31] (**Fig.1f**).

Exogenously added SCF, however, was insufficient to support ICC survival. Concentrations up to 100ng/ml of free SCF added to the culture medium failed to preserve ICC phenotype (**Fig. 1g**). There may be additional factors secreted by STO cells that are beneficial for ICC growth. When STO conditioned media (CM) was mixed into the culture medium (1:1 ratio) for MACS+ cell culture, CM provided a cell density dependent benefit to MACS+ cells. CM provided significant improvement in MACS+ cell growth on gelatin only at a lower seeding density compared to control (**Fig. 1h**). Providing CM to a low seeding density, MAC+ cells

expressed Kit to a level comparable to MACS+ cells seeded at higher density without CM (**Fig. 1h**).

The cultured MACS+ cells were passaged by performing an additional sorting on MACS+ cells growing on STO cells. Such passaged MACS+ cells (P-MACS+ cells) were seeded again on STO cells. Although the growth rate was slower, P-MACS+ cells also proliferated on STO cells and exhibited ICC morphology and expressed Kit and Ano1 (**Fig. 2a-c**).

3.3.2 Rhythmic pacemaker activity of cultured ICC (MACS+ and P-MACS+ cells)

To determine whether cells cocultured with STO cells were functional, we examined the intracellular Ca^{2+} oscillation frequency in MACS+ and P-MACS+ cells cultured on STO cells or gelatin at different density. With a higher seeding density, the MACS+ cells on STO cells exhibited a rhythmic Ca^{2+} oscillation frequency that was significantly higher than MACS+ cells cultured on gelatin (**Fig. 2d**). STO cells also supported P-MACS+ cells seeded at a higher density, and these cells exhibited a rhythmic Ca^{2+} oscillation frequency similar to MACS+ cells before passaging (**Fig. 2e**). Moreover, it's easier to maintain and restore the functionality of MACS+ cells seeded at a higher density. With a lower seeding density, it was still possible to recover the functionality of MACS+ cells, but it took a longer culture time and resulted in slightly slower frequency (**Fig. 2e**). The number of functional cells in P-MACS+ culture was about half of that in MACS+ culture due to a slower growth rate (**Fig. 2a-c**). A higher seeding density and lower passage number were beneficial for cells to form a network sooner, which lead to an earlier establishment of coordinated pacemaker activity in culture (**Fig. 2e**). Moreover, MACS+ cells cultured on STO cells demonstrated stable, periodic Ca^{2+} oscillation over time

(**Fig. 2f** and **Supplementary Video 1**). Our results suggest that the STO culture system facilitates proliferation of not only MACS+ cells but also P-MACS+ cells over time while preserving their pacemaker activities.

3.3.3 Application of MACS+ cells cultured on STO cells

ICC residing in the intestinal smooth muscle tend to align along the smooth muscle orientation[32–35] (**Supplementary Fig. 3a**). In order to induce the proper alignment, MACS+ cells were cultured on STO-seeded electrospun poly(3-caprolactone) (ePCL) scaffolds[32] (**Supplementary Fig. 3b)**. MACS+ cells proliferated and aligned along the ePCL fiber orientation after 2 weeks (**Fig. 3a**). Coherency analysis of Kit expression confirmed that MACS+ cells cultured on ePCL scaffolds (aligned) were statistically more aligned than those cultured on glass (random orientation) controls (**Fig. 3b,c**). Further, we demonstrated that MACS+ cells (GFP+) survived for at least a week *in vivo*, following colonoscopic injection into the rectal submucosa of C57BL/6 mice. Injected MACS+ cells, identified by GFP, co-localized with Ano1 expressed by ICC but not with α-SMA (**Fig. 3d,e**). Moreover, MACS+ cells were distributed around the injection site of the submucosa as indicated by carbon ink and demonstrated alignment along the smooth muscle layer, accompanied by native ICC and SMCs (**Fig. 3d,e**). These results demonstrate that the *in vitro* expanded ICC not only can be align by using scaffolds but also can survive *in vivo* through colonoscopic injections.

3.3.4 ISMC Mix maintenance on STO cells

To test whether our approach of culturing MACS+ cells with spontaneous Ca^{2+} oscillation could support periodic contractions of SMCs, ISMC Mix was cultured on STO cells for three weeks.

At day 7, ISMC Mix cultured on STO cells in F12 medium expressed the highest level of ICC markers (Kit and Ano1 co-localization), SMCs marker (MHC) and neuronal marker (β-tubulin), followed by ISMC Mix cultured on STO cells in FBS medium and ISMC Mix cultured on gelatin in FBS medium (**Fig. 4a**). Comparable to the trends observed in immunostaining, ISMC Mix on STO cells cultured in F12 medium showed the greatest expression of *Kit, Myh11, Tubb3, Kitl,* and *Acta2* up to three weeks, with the exception that cells cultured on STO cells in FBS medium had a slightly higher expression of *Kitl* at weeks two and three (**Fig. 4b**). Cells cultured on STO cells had higher expression of *Kit and Kitl* (STO-FBS vs. Ge-FBS) while F12 medium induced higher expression of *Myh11, Tubb3,* and *Acta2* (STO-F12 vs. STO-FBS) (**Fig. 4b**). Cultures with STO cells and F12 medium demonstrated the greatest expression of *Myh11* over time (**Fig. 4b**). ISMC Mix cultured on gelatin had a higher proliferation but lower expression of other markers compared to ISMC Mix cultured on STO cells with FBS or F12 medium (**Fig. 4b**). As predicted from the immunostaining and mRNA expression, ISMC Mix cultured on STO cells demonstrated periodic contractions (**Fig. 4c**) while cells cultured on gelatin in FBS medium did not contract (not shown). STO cells with F12 medium enabled ISMC Mix to retain faster frequency over a longer period of time compared to ISMC Mix cultured on STO cells in FBS medium (**Fig. 4c**). STO cells were shown to be effective in maintaining not only functional ICC but also functional ISMC. Overall, these results suggest that STO cells with F12 medium is the optimal condition to culture ISMC Mix with periodic contractions (**Supplementary Videos 2,3**).

3.3.5 Engineering functional intestinal smooth muscle

To create an implantable tissue construct for regenerative medicine, we engineered intestinal smooth muscle with proper alignment and functionality by culturing ISMC Mix on STO-seeded

ePCL in F12 medium. ISMC Mix cultured on STO-seeded ePCL demonstrated unceasing, rhythmic contraction over 10 weeks *in vitro* (**Fig. 5f**). After 10 weeks of culture, the constructs were examined with immunostaining and qPCR, demonstrating expression of ICC, SMC and neuronal markers (**Fig. 5a,b**). Although STO cells played essential roles in supporting ISMC Mix culture, the effect of STO cells likely declined over time due to its mitomycin C treatment. When STO cells were seeded alone, the reduction in the cell number and viability were observed over time (**Supplementary Fig. 4**).

To quantify the intensity and directionality of the periodic contractions generated by ISMC Mix on ePCL scaffolds, the dimensions of the most contracted scaffold was compared to those in the most relaxed scaffold. The change in area of the scaffold (**Fig. 5d**) was mainly due to a significant change in the length of the scaffold along the direction of the fibers, labelled as the height of the ePCL scaffold (**Fig. 5e**). Moreover, the cells cultured on ePCL scaffolds showed surface alignment along the direction of the fibers in the scaffold (**Fig. 5a,c**). The alignment of ISMC Mix inside the ePCL scaffolds was also quantified as we had previously described[32]. Briefly, ePCL scaffolds were cut in two orthogonal planes to expose cross section parallel or perpendicular to ePCL's aligned fibers. Coherency analysis (MHC, GFP and β-tubulin) and circularity analysis (DAPI) were used to compare the alignment in the two cross sections, where coherency factor ranges from 0 (perfect random) to 1 (perfect alignment) indicating cell alignment while circularity factor ranges from 0 (most elongated shape) to 1 (perfect circle) indicating elongation of nuclei due to cell alignment. Our results showed that the ISMC Mix cells infiltrated inside the ePCL and arranged along the ePCL's aligned fibers (**Supplementary Fig. 5**). Culturing ISMC Mix on STO-seeded ePCL produced intestinal smooth muscle

constructs with proper alignment and spontaneous rhythmic contractions (**Supplementary Video 4**).

3.3.6 ICC is essential for rhythmic contraction of ISMC Mix

To confirm the role of ICC in ISMC Mix in producing spontaneous, rhythmic contractions, MACS+ cells were separated from ISMC Mix to create a MACS- cells population that contains few ICC. The MACS- cells were cultured on STO cells for 3 weeks *in vitro*, and its motility, gene and protein expression were analyzed. The comparison between passaged ISMC Mix (MACS0) and MACS- cells showed that the ICC population in MACS0 is essential for spontaneous rhythmic contractions (**Fig. 6a-c**). MACS- cells, without an ICC population, failed to exhibit rhythmic contractions even though SMCs and neuronal cells were present. We also performed a rescue experiment where MACS+ cells were added back to MACS- cells 5 days after they were cultured on STO cells (MACS-/+).The added MACS+ cells restored the rhythmic contractions of the MACS- cells cultured on STO cells in 5 weeks (**Fig. 6d-f)**. This experiment confirms that ICC play an essential role in producing the spontaneous rhythmic contractions of cultured ISMC.

3.4 DISCUSSION

This study demonstrates that STO cells can support ICC in culture and maintains the spontaneous intracellular Ca^{2+} oscillation frequency within the previously published range[16,18,26,36–41]. These functional ICC pace the rhythmic contractions of SMC. It is also necessary for SMC to retain its maturity and express MHC to contract[12,13] upon receiving pacemaker signals from functional ICC. The loss of maturity and functionality of either ICC or

SMC in culture is a major challenge for intestinal smooth muscle engineering[12,13,42]. Our system described here is the first approaches to achieving this goal by maintaining the functionality of both ICC and SMC, as well as neuronal cells cultured *in vitro*.

This system provides an easily accessible *in vitro* model to investigate the molecular mechanisms underlying a functional smooth muscle. The combination of STO cells and F12 medium works well to produce the *in vitro* culture of the intestinal smooth muscle. While it is likely that STO cells provide signals including preferable forms of SCF [43,44] and other factors[31] important for ICC to survive and function, the exact mechanisms that underlie these observations will need to be investigated further. The beneficial effects provided by STO cells are important during the initial phase of the smooth muscle cell culture. It is likely that other cell types within ISMC Mix eventually take over the function of STO cells due to the mitomycin C treatment.

This novel culture method is likely to have broad applications. We demonstrated that both MACS+ cells and ISMC Mix were able to attach and align along ePCL scaffolds and that MACS+ cells cultured using our system survived *in vivo* after colonoscopic injections. Specifically, colonoscopic injections of ICC may help motility disorders including diabetic gastroparesis, pseudo-obstruction and Hirschsprung's disease due to frequent defects in ICC networks reported in those disorders[29,30]. The culture method could also be applied to cells from other visceral organs[45], and the cultured cells could be seeded on other biomaterials, used in other *in vivo* studies, and incorporated into microfluidic systems.

Finally, this culture system is simple and reproducible for generating a functional smooth muscle layer *in vitro*. Our STO cell system only requires standard culture medium without specialized additives. STO cells are readily available at a low cost from commercial vendors. We believe that the STO cell system has the potential to become a common method to create

functional smooth muscle *in vitro.* This system may serve as the platform for both basic and applied research in intestinal motility.

3.5 METHODS

3.5.1 Electrospinning. 11% (w/w) solution of PCL (Durect Lactel, Birmingham, AL) was made in hexafluoro-2-propanol (Acros Organics, Thermo Fisher Scientific, Waltham, MA). The solution was kept on a shaker overnight to obtain a homogenous polymer solution. The mandrel was wrapped with aluminum foil to ease the removal of the scaffold. The PCL solution was transferred to a plastic syringe fitted with an 18-gauge needle, and secured onto a syringe pump (Harvard Apparatus, Holliston, MA). The solution was infused at 2.5 ml/h onto a rotating mandrel collector with an outer diameter of 32 mm that was positioned 12-15 cm away from the needle tip. The electrical potential difference between the needle (i.e., polymer solution) and the grounded mandrel collector was produced by a high voltage power supply (Glassman High Voltage, High Bridge, NJ). Scaffolds comprised of aligned ePCL fibers were fabricated using a mandrel rotational speed of 3450 rpm and an applied voltage of 15 kV. Less-aligned, “random” ePCL fibers were produced using a mandrel rotational speed of 1725 rpm and applied voltage of 25 kV. After 0.5 ml of polymer solution had been dispensed from the syringe onto the rotating mandrel, the ePCL was carefully removed from the aluminum foil. Scaffolds were air-dried before laser cutting.

3.5.2 Laser cutting. ePCL scaffolds were constructed as fiber sheets with dimensions approximately 10 x 2.5 cm and thickness of 100-150 μm, based on the mandrel used. These fiber sheets were cut into rectangular 8 x 6.5 mm scaffolds using the VERSA LASER CUTTER 2.3

(Universal Laser Systems, Scottsdale, AZ) with vector mode, 5% power, 100x speed, and 1000 pulses/inch. Scaffolds were obtained by setting the longer edge of the rectangle to be along the fiber direction. The scaffolds were cleaned with air plasma (Harrick Plasma, Ithaca, NY) at 500 mTorr, high power for 1 min and subsequently sterilized with strong UV (Dymax) for 1min. The scaffolds were washed once with phosphate buffered saline (PBS) (Invitrogen, Carlsbad, CA) before and after coating with gelatin solution (attachment factor solution (AF); Invitrogen) at 37°C for at least 30 min. (Note: To improve the cell seeding onto ePCL scaffolds, PDMS molds with a well size the same as an ePCL scaffold were manufactured. This will allow ePCL scaffold to fit perfectly and stay at bottom of the PDMS well so that seeded cells attached effectively on the ePCL scaffold with minimal spillage to the bottom of the well).

3.5.3 Scanning Electron Microscopy (SEM). The surface morphology of ePCL scaffolds with aligned or random fibers was assessed using a Nova NanoSEM 230 (FEI, Hillsboro, Oregon). The scaffolds without conductive coating were mounted on the sticky conductive carbon tape (Ted Pella, Redding, California) on the top of aluminum stubs (Ted Pella, Redding, California) and examined under SEM with an accelerating voltage of 10 kV at low vacuum mode.

3.5.4 Ethics statement. Animal usage complied with regulations set by the University of California, Los Angeles, Chancellor's Animal Research Committee and was approved as animal protocol number 2005-169. All efforts were made to minimize pain and suffering. Two mice strains were used for these experiments: C57BL/6-Tg(Actb-EGFP)1Osb/J ("GFP") (The Jackson Laboratory, Bar Harbor, ME) and wild type C57BL/6 (Charles River, Wilmington, MA).

3.5.5 Feeder cells preparation. Embryonic fibroblasts, STO (SIM, Santos Inbred Mouse) and MEF (C57BL/6) (both from ATCC) were expanded in STO medium (low glucose DMEM with GlutaMAX^{TM} supplemented with 10% FBS and 1x ABAM (All Invitrogen)) and suspended in STO medium with 10% DMSO for cryopreservation (~10^6 cells/ml, 1ml/vial). ~10^6 feeder cells were thawed and cultured in gelatin coated T25 flasks with STO medium for a few days until confluency and treated with mitomycin C (Sigma). ~100k cells were seeded onto gelatin-coated substrates such as 48-well plate (Coring Costar, Fisher Scientific), eight-chamber slide (Nunc™ Lab-Tek™ II; Thermo Scientific) and ePCL scaffold, and cultured at 37°C with STO medium in a 10% CO_2 incubator. Prepared feeder cells were used within 3 days.

3.5.6 Primary intestinal smooth muscle cell mixture (ISMC Mix) isolation and culture. ISMC Mix were isolated from 7 to 10-day-old C57BL/6 neonates using previously described methods [12,32,36,46]. The intestines were removed via a midline incision, and smooth muscle strips, containing both longitudinal and circular muscle layers, were gently teased from the intestines using fine forceps and placed in Hank's Balanced Salt Solution (HBSS) without calcium and magnesium (Invitrogen, Carlsbad, CA) with 1x antibiotic-antimycotic (ABAM) (Invitrogen) on ice. Then the smooth muscle strips were minced and incubated at 37°C for 30~40 min in an enzyme solution containing collagenase (1.3 mg/ml Worthington Type II; Worthington Biochemical, Freehold, NJ), bovine serum albumin (BSA) (2 mg/ml), trypsin inhibitor (2 mg/ml), ATP (0.27 mg/ml) (all from Sigma, St. Louis, MO), and 10% HBSS with calcium and magnesium (Invitrogen) in HBSS without calcium and magnesium containing 1x ABAM. The tissue was washed twice with vigorous pipetting with 10% FBS in HBSS without calcium and magnesium containing 1x ABAM. As a preparation for immunomagnetic sorting (MACS), the

resulting ISMC Mix was cultured in gelatin coated T25 flasks (ISMC Mix from ~4 pups in one T25 flask) for 3 days. Alternatively, 100k ISMC Mix were seeded onto substrates (48 well plate, eight-chamber slide, ePCL scaffold) with STO cells or gelatin coating. ISMC Mix were cultured at 37°C in a 5% CO_2 incubator in FBS medium (Knockout™ D-MEM supplemented with 15% ECS-qualified FBS, 0.1 mM MEM Non-Essential Amino Acids solution, 2 mM L-glutamine, 0.1 mM 2-mercaptoethanol, 1x ABAM, and 10mM HEPES (Invitrogen)). All ISMC Mix were cultured in FBS medium for the first 4 days followed by FBS or F12 medium (Advanced DMEM/F-12 supplemented with 2 mM L-glutamine, 1x ABAM, and 10mM HEPES (Invitrogen)). For conditioned medium (CM) preparation, STO medium was replaced with FBS medium after the STO cells formed a confluent monolayer and treated with mitomycin C. The FBS medium was collected after 4~5 days of incubation, passed through a 0.2 μm pore size filter (Pall Corporation, Port Washington, NY), and mixed with fresh FBS medium (1:1 ratio) as CM. The medium was changed every 2~3 days.

3.5.7 Enrichment of ICC by immunomagnetic sorting (MACS). After 3 days in culture, ISMC Mix were washed in PBS and incubated with 0.05% trypsin-EDTA (Invitrogen) at 37C for ~2 min The ICC marker, Kit, the epitope recognized by ACK2, is easily altered or masked during the enzymatic digestion process. Therefore, it is important to avoid over-digestion. The reaction was stopped by adding FBS medium. The dissociated cells were washed once with sorting buffer (1% BSA (Fisher Scientific) and 2mM EDTA (Sigma) in PBS; ~pH7.2) and passed through a 100 μm cell strainer (Fisher Scientific). After centrifuging the cell suspension at 1000 rpm for 5 min, supernatant was aspirated completely. The cell pellet was re-suspended in sorting buffer and then well-mixed with the CD117 MicroBeads solution (Miltenyi Biotec,

Germany; 1:5 in sorting buffer). The cell suspension was incubated for 15 minutes at 4°C. For cells from four pups, 160 µL of sorting buffer and 40 µL of CD117 MicroBeads solution were used. Half the volume was used for cells isolated from two pups. The cell suspension was mixed with pipetting every 5 min. After being washed twice with the sorting buffer, the labeled cells were re-suspended in sorting buffer and 0.5 ml of the cell suspension was passed through pre-wetted MS magnetic columns placed in a strong magnet (MiniMACS; Miltenyi Biotec) at a time. Cells from four pups were re-suspended in 4 ml sorting buffer and passed through two MS columns, 2 ml per each. After passing all of the cell suspension, MS columns were washed once with 1 ml of sorting buffer. Unlabeled cells were collected as flow-through (MACS- cells), while labeled cells retained in the columns were flushed out with 1 ml of sorting buffer after removing the column from the magnet (MACS+ cells). MACS+ cells were seeded onto gelatin or feeder cells and cultured at 37°C, 10% CO_2 incubator in FBS medium.

For P-MACS culture, the resultant MACS+ cells from 4 pups were all cultured on a STO-seeded well of a 6-well plate for 7 days, passaged with MACS, and subsequently cultured on STO cells in FBS medium. The medium was changed every 2~3 days.

For MACS0, MACS- and MACS-/+ culture, CD117 MicroBeads labeled cells without passing through the MS magnetic column (MACS0) and MACS- cells were cultured on STO cells in FBS medium for 4 days followed by F12 medium. We also added MACS+ cells back to MACS- cell culture 5 days after they were cultured on STO cells in order to recover its spontaneous contractility (MACS-/+). The MACS-/+ cells were cultured in FBS medium for 7 days, followed by F12 medium (2 days after adding the MACS+ cells onto MACS- cells). The medium was changed every 2~3 days.

3.5.8 Measurement of pacemaker activity in purified ICC (MACS+ cells). To monitor oscillations in intracellular Ca^{2+} concentration, cultured ICC (MACS+ cells) were incubated with 1 part of 2X Fluo-4 Direct™ calcium reagent loading solution without probenecid (Invitrogen) and 1 part of FBS medium at 37°C, 5% CO_2 incubator for 0.5~1 hour. Incubating for too short of a time will result in a weak signal while too long will result in an increased number of floating dead cells. Fluorescent images (680x512 pixels) were acquired with an Olympus IX71 microscope using cellSens software (Olympus, Center Valley, PA) (acquisition rate: 4.8~7.7Hz; excitation wavelength: 494 nm; emission wavelength: 516 nm), and analyzed using custom MATLAB programs[12] (region of interest analysis, **Supplementary Fig. 6;** fast-forward and gray scale normalization, **Supplementary Fig. 7**). In order to keep the temperature close to 37°C[47,48], cells were limited to 5 min at room temperature for image acquisition and were returned to the incubator before repeating the process.

3.5.9 Colonoscopic injection of MACS+ cells cultured on STO cells. Eight to 12 week old male and female C57BL/6J mice (n=3) were placed on water only diet overnight. Anesthesia was induced with 3% isoflurane then decreased to 1% for maintenance. Colonoscopy was performed by introducing a lubricated 1.9 mm endoscope (Karl Storz, Tuttlingen, Germany) into the mouse rectum, as previously described[49]. GFP+ MACS+ cells were cultured on STO cells for 4 days and MACS purified prior to the colonoscopic injection. The resulting P-MACS+ cells were re-suspended in low glucose DMEM with GlutaMAX™ (Invitrogen) to a concentration of $5x10^5$ cells/ml and mixed with 1.5% permanent carbon ink (Spot; GI Supply, Camp Hill, PA) for later identification of the injection sites. Using a 30 gauge custom-made needle fitted with pulled and beveled capillary tubing[49], 100 µL of the cell suspension was injected into the submucosa of the

ventral rectum (n= 12 total). Mice were monitored for appropriate recovery from anesthesia and placed back in standard laboratory mouse cages with full access to water and chow. All mice were sacrificed 7 days after the cell injection procedure and colon specimens were isolated.

3.5.10 Histology & immunofluorescence staining. Samples, including cell-seeded ePCL and P-MACS+ injected intestine, were formalin-fixed and processed for paraffin embedding. Serial 5 µm sections were cut and adhered to glass slides. Unstained slides were prepared for immunofluorescence staining. Slides were de-waxed with xylene and rehydrated with serial dilutions of ethanol. Next, slides were incubated in a citric buffer (Biogenex, San Ramon, CA) for 15 min at 95-100°C and allowed to cool for 15 minutes in an over flowing water bath. *In vitro* cultures and native smooth muscle strips were fixed without histologic processing. For Kit and Ano1 staining, samples were fixed with acetone for 30 min at 4°C. For all the other staining, samples were fixed with 10% formalin for 30 min at room temperature. After three washes with PBS, samples were treated with a blocking buffer containing 5% normal goat serum (Vector Labs, Burlingame, CA), 0.1% Triton X-100 (Sigma) in PBS for 1 hour at 4°C. Samples were then incubated with the following primary antibodies: Kit (1:500; eBioscience: 16-1172-82), Ano1 (1:500; Abcam: ab53212), MHC (1:100; Abcam: ab53219), β-tubulin (1:500; Abcam: ab78078), GFP (1:500; Aves: GFP-1020), and SCF (1:500; ab64677) diluted in staining buffer containing 5% normal goat serum in PBS overnight at 4°C. After two washes in PBS, samples were incubated in the dark with their corresponding Alexa Fluor® secondary antibodies (1:500; Invitrogen) and Alexa Fluor® 594 Palloidin (1:100; Invitrogen) diluted in staining buffer for 2~3 hours at room temperature. After three washes with PBS, Prolong Gold with DAPI (Invitrogen) was applied to each section and the slides were covered with glass coverslips. The

slides were allowed to cure at 4°C before storing at -80°C. Fluorescent images were acquired with an Olympus IX71 microscope with cellSens software (Olympus, Center Valley, PA) or confocal laser microscopy (TCS SP2 AOBS, TCS SP2 MP AOBS; Leica).

3.5.11 DNA/RNA extraction and qPCR. DNA and RNA were extracted and purified from *in vitro* cultures using the DNeasy and RNeasy kits (Qiagen, Valencia, CA), respectively following the manufacture's protocol. RNA samples were cleaned with RNase-Free DNase set (Qiagen) during the procedure. The qPCR reactions were prepared using a PCR master mix and the Quantitect Probe RT-PCR Kit (Qiagen) and performed on an ABI 7500 Real Time PCR System (Applied Biosystems). The primers and probe for *gfp*-DNA and *Kit*-RNA were custom- designed and purchased from Eurofins MWG Operon, (Huntsville, AL) : *gfp*-fw, 5'-ACTACAACAGCCACAACGTCTATATCA-3'; *gfp*-rev, 5'-GGCGGATCTTGAAGTTCACC-3'; *gfp*-pb, and 5'-[6-FAM]CCGACAAGCAGAAGAACGGCATCA[TAMRA-Q]-3'; *Kit*-fw, 5'-CCGTGAACTCCATGTGGCTAAAGA; *Kit*-rev, 5'-GGTGCCAGCTATTGTGCTTTACCT-3'; *Kit*-pb, 5'-[6-FAM]TGAACCCTCAGCCTCAGCACATAGC[TAMRA-Q]-3'. All the other primer/probe mixtures were purchased from Applied Biosystems: *Myh11* (Mm00443013_m1), *Tubb3* (Mm00727586_s1), *Kitl* (Mm00442972_m1), *Acta2* (Mm01546133_m1), *Ano1* (Mm00724407_m1) and *Gapdh* (Mm99999915_g1). DNA qPCR results were analyzed using a standard prepared with known number cells from ISMC Mix. RNA qPCR results were analyzed using *Gapdh* as the housekeeping gene and de-epithelialized intestine as reference.

3.5.12 MTS assay. MTS assay was conducted to test the viability of mitomycin C treated STO cells over time. 100k mitomycin C treated STO cells were seeded on to 48-well plate in STO

medium overnight, followed by the same series of medium as the preparation for ISMC Mix feeder layer. At each time point, wells with cells and without cells (control) were incubated with a mixture of CellTiter 96® AQueous One Solution Reagent (Promega) in appropriate medium (1:5 volume ratio) at 37°C in a 5% CO_2 incubator for an hour. The absorbance was measured at 490 nm (Synergy^{TM} HT; BioTek). Data were normalized to controls.

3.5.13 Data Analysis. The frequency of spontaneous contractions of the cells was analyzed manually from recorded videos (680x512 pixels; acquisition rate: 5.0 Hz) acquired with an Olympus IX71 microscope using cellSens software (Olympus, Center Valley, PA). The area, height and width of the most contracted ePCL scaffolds were normalized to that of the most relaxed ePCL scaffolds with ImageJ using images extracted from a representative video and manually outlined ePCL scaffolds. In order to compare the size of feeder cells, area of MEF was normalized to that of STO cells with ImageJ. For the cell alignment quantification, ImageJ was used to conduct circularity analysis (DAPI) and the plugin OrientationJ was used to conduct coherency analysis (Kit, MHC, GFP and β-tubulin).

3.5.14 Statistical Analysis. One-way ANOVA followed by Tukey test or two-tailed unpaired Student's t-test was used depending on the number of simultaneous conditions to analyze. Levels of significance were set at *** $P < 0.0001$, ** $P < 0.01$, and * $P < 0.05$. Data were expressed as the mean ± the standard deviation (s.d.). n indicates the number of independent experiments (different primary cell isolations from different animals) except for the following cases: Fig. 2de, n = number of cell cultures (from 3 different independent experiments); Fig. 3c, n = number of images (from one independent experiment); Fig. 4c, n = number of videos (from two

independent experiments); Fig. 5de, n = number of images (extracted from a representative video).

3.6 ACKNOWLEDGEMENTS

Confocal laser scanning microscopy was performed at the CNSI Advanced Light Microscopy/Spectroscopy Shared Resource Facility at UCLA. We thank Dr. Matthew Schibler for his generous help with the facility. We also thank UCLA Translational Pathology Core Lab for histologic processing. This work was funded by R01 DK083119 from the National Institutes of Health.

3.7 FIGURES

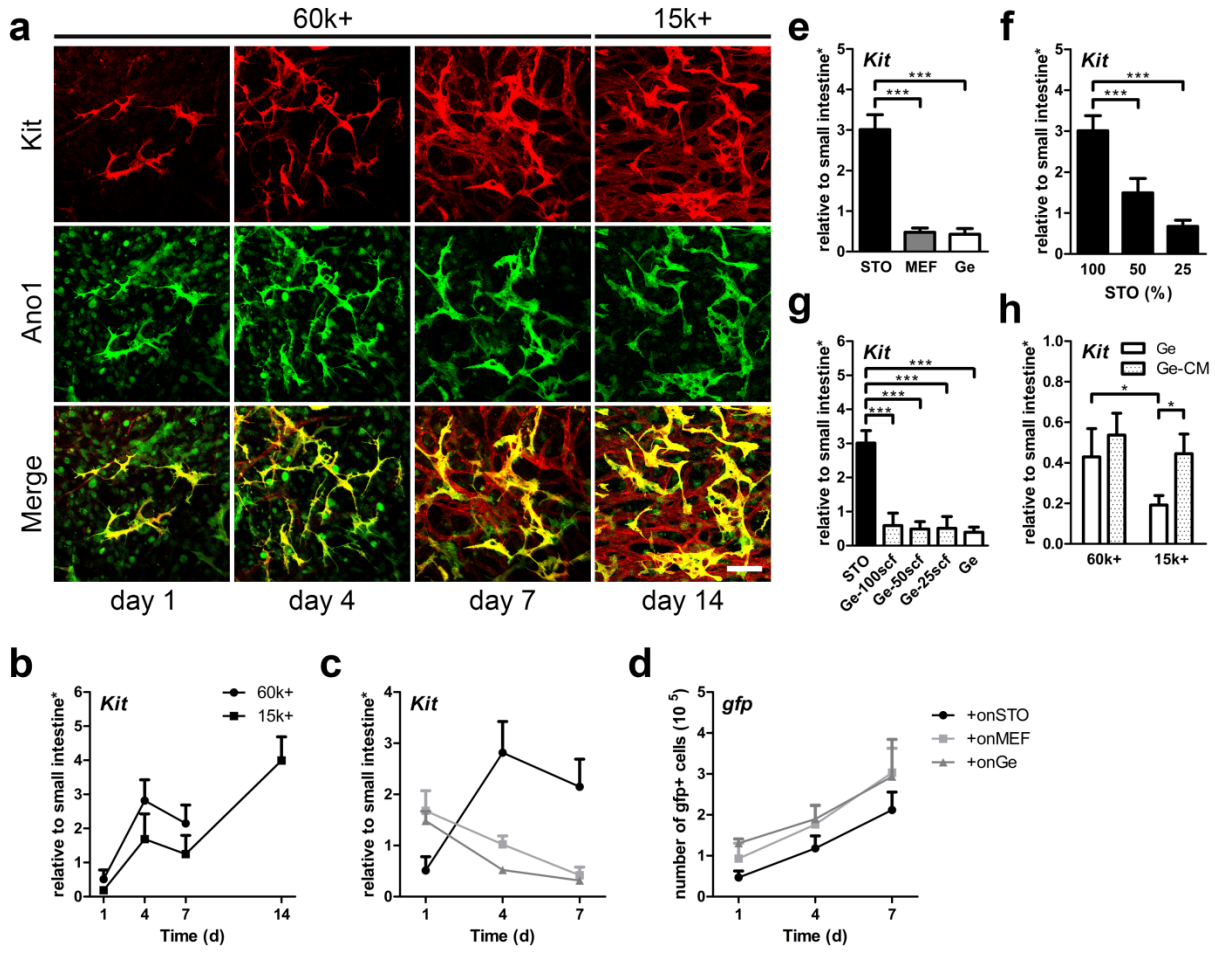

Figure 1 | Maintenance of MACS+ cells cultured on STO cells. (**a**) Confocal images of ICC markers, Kit (red), Ano1 (green), and co-localization (yellow). 60k MACS+ and 15k MACS+ cells were cultured for 7 days and 14 days respectively. Scale bar, 100 µm. (**b**) MACS+ cells were analyzed for Kit mRNA expression (**b-d**: day 1, 4, 7 *n=4*; day 14 *n =2*). (**c-d**) GFP+ MACS+ cells were seeded on STO cells, MEF, and Ge, cultured, and analyzed for mRNA expression of *Kit* (**c**) and *gfp* DNA (**d**). STO cells and MEF do not express *Kit/gfp*. (**e**) mRNA expression of *Kit* for MACS+ cells cultured on STO cells, MEF and Ge for 7 days. (**f**) mRNA expression of *Kit* for MACS+ cells cultured on different STO seeding densities for 7 days, where 100% is 100k (100%, *n=5;* 50%, *n=4;* 25%, *n=2*). (**g**) mRNA expression of

Kit for MACS+ cells cultured on Ge for 7 days in media supplemented with 25, 50, or 100 ng/ml of soluble scf (*n=2*). STO and Ge were controls (*n = 5*). (**h**) mRNA expression of *Kit* for 60k or 15k MACS+ cells cultured on Ge for 7 days supplemented with conditioned media from STO (Ge-CM), where Ge was the control (*n= 4*). STO = Mouse Embryonic Fibroblast (Santos Inbred Mouse, SIM). MEF = Mouse Embryonic Fibroblast (C57BL/6). Ge = gelatin coating. Feeder cells (STO, MEF) were mitomycin C treated. *Samples were normalized to de-epithelialized intestine. Error bars, s.d. *** $P < 0.0001$, * $P < 0.05$.

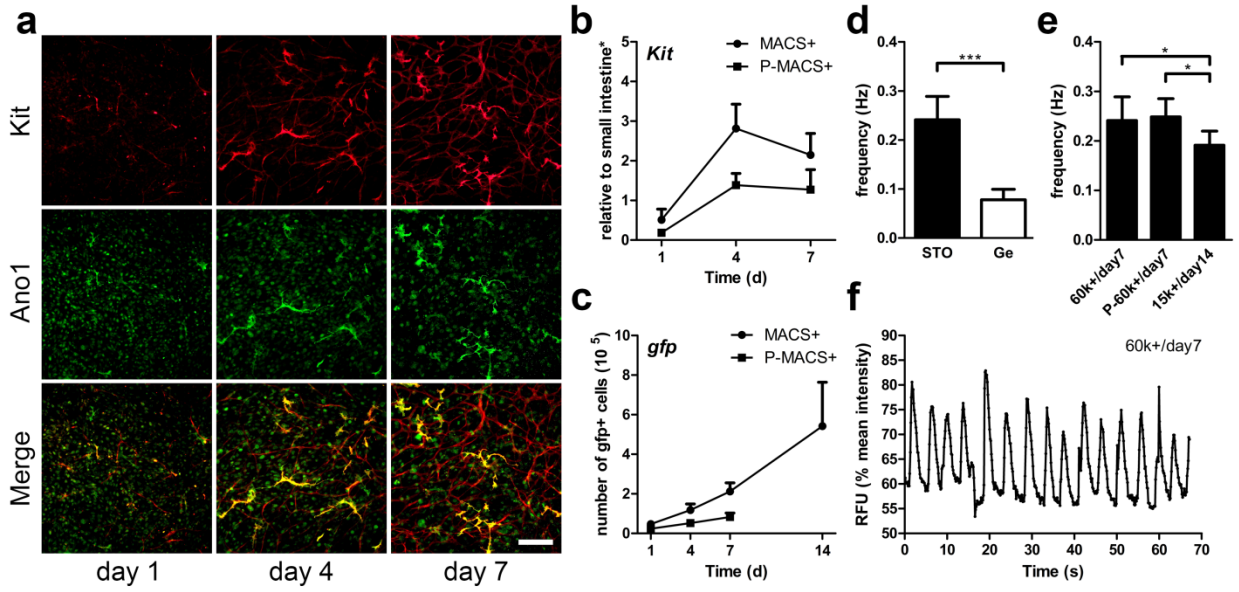

Figure 2 | Maintenance of passaged MACS+ cells on STO cells and rhythmic pacemaker activity of cultured ICC (MACS+ and passaged MACS+ cells). 60k sorted cells were cultured for 7 days unless otherwise noted. (**a**) Immunofluorescence of passaged MACS+ (P-MACS+) cells with ICC markers, Kit (red) and Ano1 (green) and with co-localization (yellow). MACS+ cells were cultured on STO cells for 7 days and were passaged and sorted with MACS (P-MACS+). P-MACS+ cells were subsequently cultured on STO cells. Scale bar, 200 µm. (**b-c**) Growth comparison of GFP+ MACS+ and P-MACS+ cells with mRNA expression of *Kit* (**b**) and DNA expression of *gfp* (**c**). (**b-c**: day 1, 4, 7 *n=4*; day 14 *n =2*). (**d-f**) Oscillations in intracellular Ca^{2+} concentration demonstrated the rhythmic pacemaker activity in MACS+ and P-MACS+ ICC cultures and their frequency were measured. (**d**) Ca^{2+} oscillation frequency of MACS+ cells cultured on STO cells or Ge at day 7 ($n \geq 5$). (**e**) Ca^{2+} oscillation frequency of 60k MACS+ and 60k P-MACS+ cells cultured on STO cells at day 7, and the frequency of 15k MACS+ cells cultured on STO cells at day 14 ($n \geq 5$). (**f**) Representative time-course change in fluorescence intensity due to Ca^{2+} oscillation of ICC in the culture of MACS+ cells on STO cells at day 7 (**Supplementary Video 1**). *Samples were normalized to de-epithelialized intestine. Error bars, s.d. *** $P < 0.0001$, * $P < 0.05$.

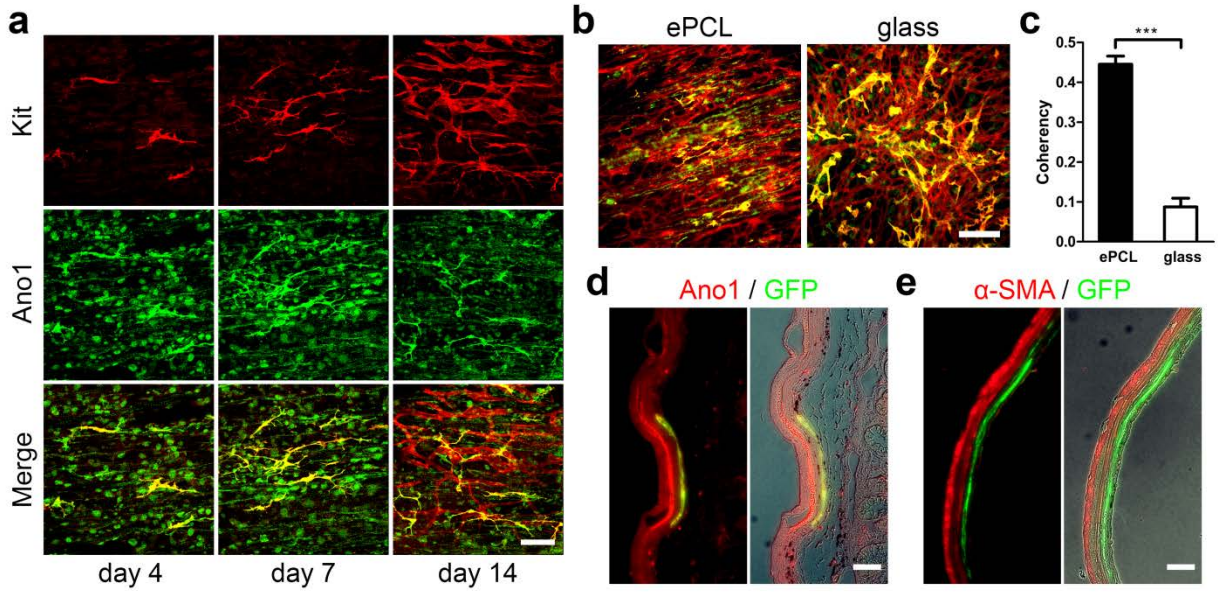

Figure 3 | Application of MACS+ cells cultured on STO cells. (**a**) Confocal images of ICC markers, Kit (red), Ano1 (green), and co-localization (yellow). 15k MACS+ cells were cultured on STO-seeded ePCL scaffold for 14 days. Scale bar, 100 µm. (**b-c**) Quantification of Kit alignment expressed by 15k MACS+ cells cultured on STO-seeded ePCL and glass for 14 days. (**b**) Immunofluorescence of ICC markers, Kit (red) and Ano1 (green) and with co-localization (yellow). Scale bar, 200 µm. (**c**) Coherency analysis of Kit expression of MACS+ cells cultured on ePCL(aligned) and glass (random), where higher coherency means greater cell alignment (*n=5*). (**d-e**) GFP+ MACS+ cells were cultured on STO cells for 4 days and purified using MACS before colonoscopic injection into the submucosa of the rectum of C57BL/6 mice. A permanent carbon ink was mixed into the cell suspension to mark injection sites. The injected rectums were retrieved after 7 days, and were immunostained for Ano1 (**d**, red), α-SMA (**e,** red) and GFP (**d, e,** green). GFP co-localized with Ano1 (**d,** yellow) but not with α-SMA (**e**). Merged immunofluorescence images (left) were further merged with phase contrast images to show the area of injection indicated by black ink (right). Scale bar, 100 µm. Error bars, s.d. *** $P < 0.0001$.

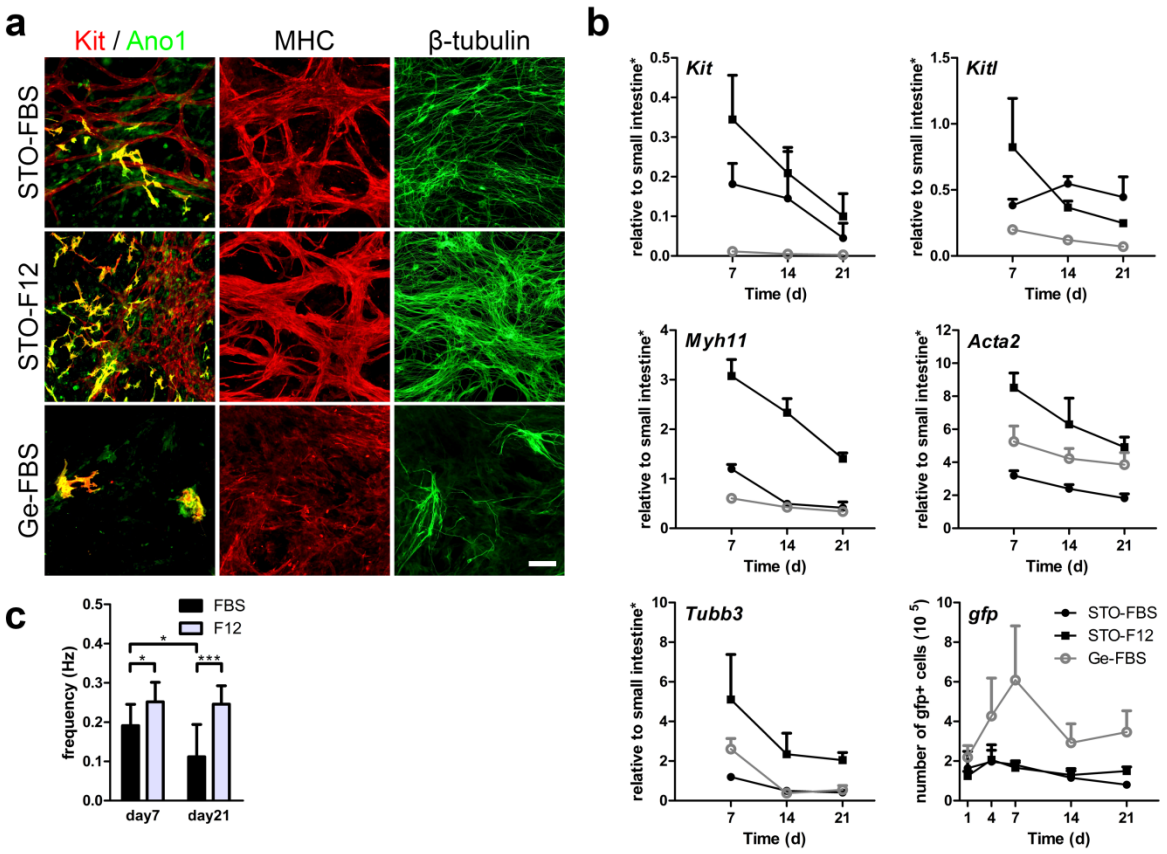

Figure 4 | Maintenance of intestinal smooth muscle cell mixture (ISMC Mix) cultured on STO cells *in vitro* over time. Non-sorted cells from enzymatically digested intestinal muscle strips were used. All ISMC Mix were cultured in FBS medium for the first 4 days followed by FBS or F12 medium. (**a-c**) 100k ISMC Mix were cultured on STO cells or Ge with FBS or F12 medium for up to 3 weeks. (**a**) Immunofluorescence of ISMC Mix with ICC markers showing co-localization (yellow) of Kit (red) and Ano1 (green), SMCs marker MHC (red), and neuronal marker β-tubulin (green) at day 7. Scale bar, 100 μm. (**b**) GFP+ ISMC Mix were analyzed for mRNA expression (*Kit*, *Myh11*, *Tubb3*, *Kitl*, and *Acta2*) and *gfp* DNA ($n=3$). (**c**) Spontaneous contraction demonstrated the functionality of ISMC Mix cultured on STO cells with FBS or F12 medium (**Supplementary Video 2,3**) and frequency was measured ($n \geq 5$). FBS = 15% FBS in DMEM. F12 = advanced DMEM/F12. *Samples were normalized to de-epithelialized intestine. Error bars, s.d. *** $P < 0.0001$, * $P < 0.05$.

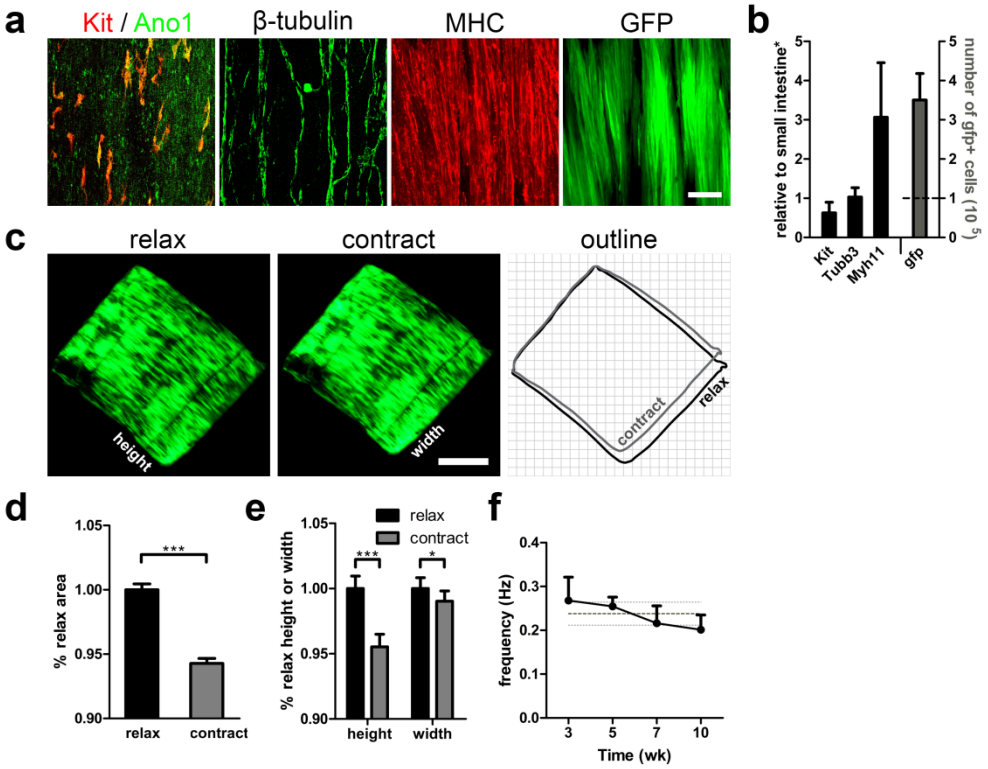

Figure 5 | Engineering aligned intestinal smooth muscle with periodic contraction over 10 weeks *in vitro*. 100k ISMC Mix were cultured on STO cells seeded ePCL scaffolds in FBS medium for the first 4 days before changing to F12 medium. (**a**) Confocal images of ISMC Mix with ICC markers showing co-localization (yellow) of Kit (red) and Ano1 (green), SMCs marker MHC (red), neuronal marker β-tubulin (green), and GFP (green) at 10 weeks. Scale bar, 100 μm. (**b**) GFP+ ISMC Mix were analyzed for mRNA expression (*Kit*, *Myh11*, *Tubb3*, *Kitl*, and *Acta2*) (*n=5*) and *gfp* DNA (*n=4*). The dashed line indicates the seeding density. (**c-e**) Relaxed and contracted state comparison of engineered intestinal smooth muscle. (**c**) Images of GFP expression from ISMC Mix seeded ePCL scaffold were extracted from a video recording and outlined (relax, black; contract, gray) for comparison. Scale bar, 2mm (**Supplementary Video 4**). (**d)** To show the degree of the periodic contraction, area of contracted ePCL scaffolds were normalized to that of relaxed ePCL scaffolds (*n = 10*). (**e)** To show the directionality of the periodic constriction, height and width of contracted ePCL scaffolds were normalized to those of relaxed ePCL

scaffolds (*n = 10*). (**f**) Frequency of ePCL rhythmic contractions (*n = 4*). The dark gray dashed line indicates the mean frequency over time and light gray dashed lines indicate its s.d. *Samples were normalized to de-epithelialized intestine. Error bars, s.d. *** $P < 0.0001$, * $P < 0.05$.

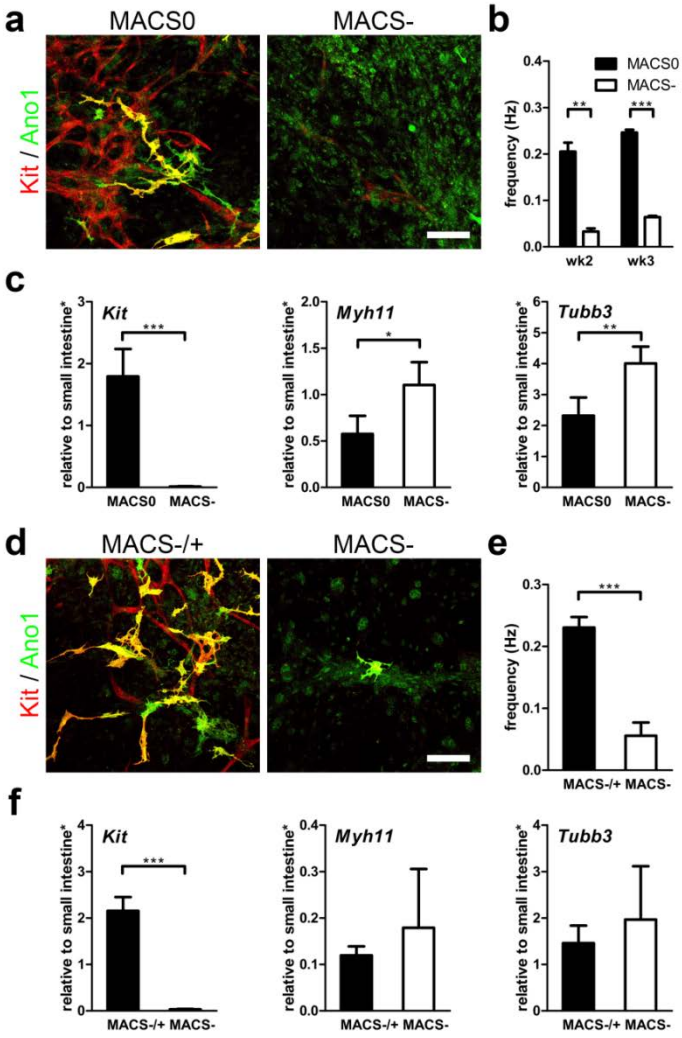

Figure 6 | MACS+ cells' role in cultured ISMC Mix with rhythmic contractions *in vitro*. (**a-c**) 100k MACS0 (passaged ISMC Mix: mixture of MACS+ cells, SMCs and neuronal cells) or MACS- cells (ISMC Mix without MACS+ cells: mostly SMCs and neuronal cells) were cultured on STO cells for 3 weeks. Cells were seeded and cultured in FBS medium for the first 4 days before changing to F12 medium. (**d-f**) 100k MACS- were seeded on STO cells for 5 weeks, with (MACS-/+) or without (MACS-) addition of 60k MACS+ cells on day 5. Cells were cultured in FBS medium for the first 7 days before changing to F12 medium. (**a, d**) Confocal images of ICC markers, Kit (red), Ano1 (green), co-localization (yellow). Scale bar, 100 μm. (**b, e**) Frequency of cultured cells motility due to spontaneous contraction (**b**:

wk2 *n=2*, wk3 *n=4*; **e**: wk5 *n=4*). (**c, f**) Cultured cells were analyzed for mRNA expression (*Kit, Myh11, Tubb3*) at week 2 (**c**) or week 5 (**f**) (*n=4*). *Samples were normalized to de-epithelialized intestine. Error bars, s.d. *** $P < 0.0001$, ** $P < 0.01$, * $P < 0.05$.

3.8 SUPPLEMENTARY FIGURES

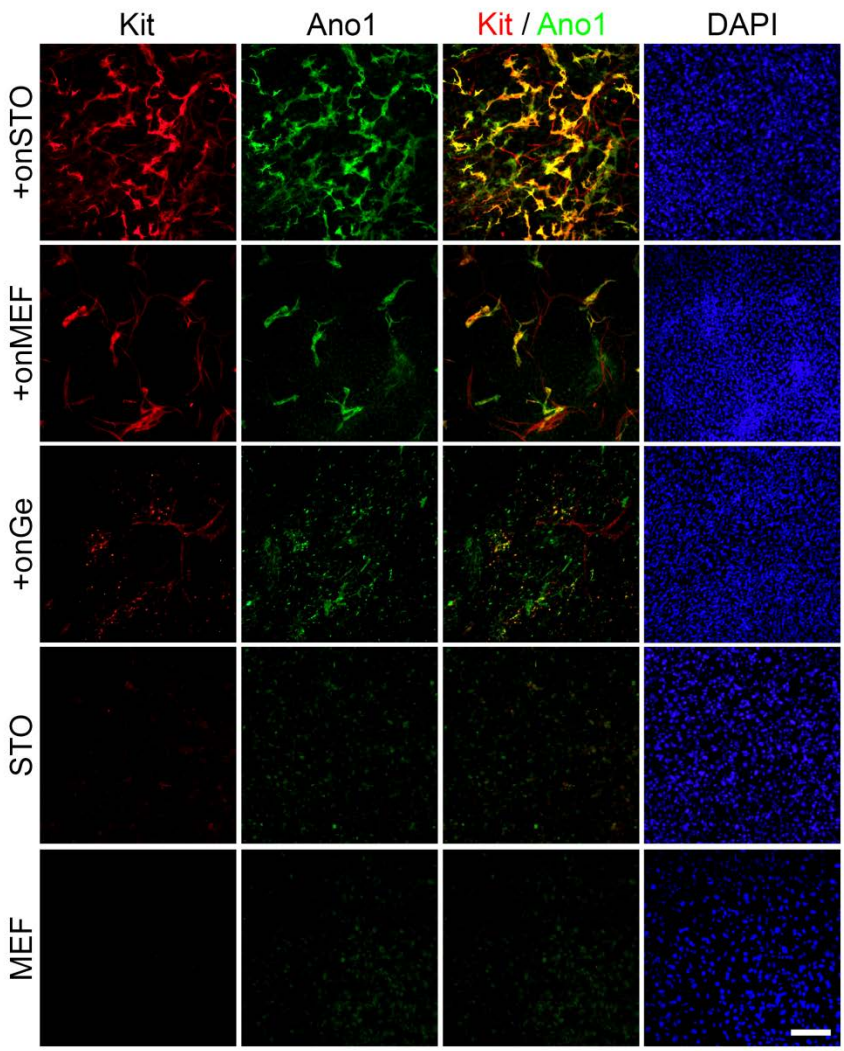

Supplementary Figure 1 | Comparison of MACS+ cells cultured on STO cells, MEF cells, and gelatin *in vitro*. Immunofluorescence of ICC markers: Kit (red) and Ano1 (green) and with co-localization (yellow), and nuclear marker DAPI (blue). 60k MACS+ cells on different substrates and feeder cells alone (STO, MEF: controls) were cultured for 7 days. Scale bar, 200 µm. STO = Mouse Embryonic Fibroblast (Santos Inbred Mouse, SIM). MEF = Mouse Embryonic Fibroblast (C57BL/6). Ge = gelatin coating. Feeder cells (STO, MEF) were mitomycin C treated.

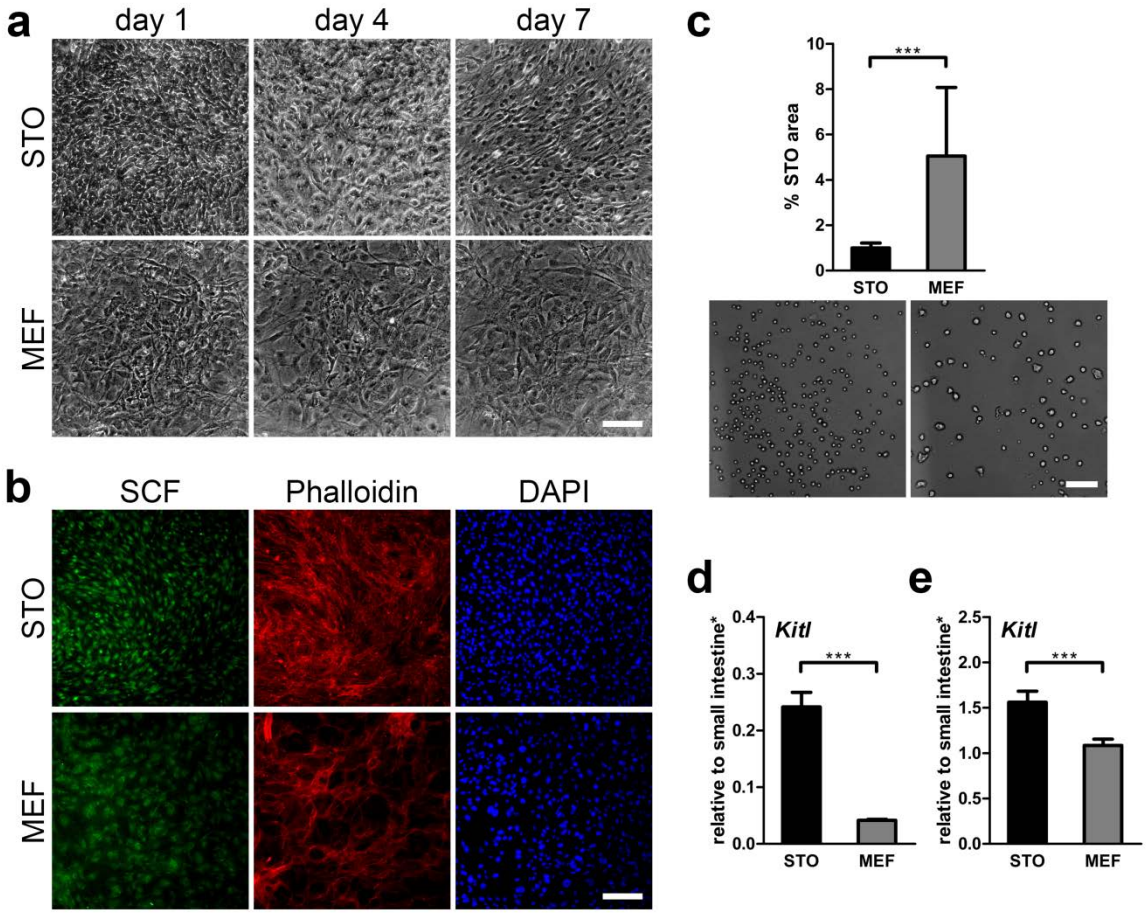

Supplementary Figure 2 | Comparison of STO and MEF feeder cells cultured *in vitro* over time. 100k feeder cells were seeded on gelatin in STO medium overnight and cultured in FBS medium for 7 days. (a) Phase contrast images of the feeder cells. Scale bar, 100 µm. (b) Immunofluorescence of feeder cells with Kit ligand marker SCF (green), cytoskeleton marker phalloidin (red), and nuclear marker DAPI (blue). Scale bar, 200 µm. (c) Comparison of the size of feeder cells suspended in medium at day 0 before seeding. Phase contrast images were taken for cell area comparison. Area of MEF cells were normalized to that of STO cells (*n=70* cells; *** $P < 0.0001$). Scale bar, 100 µm. (d-e) Feeder cells were compared for their *kitl* mRNA expression at day 0 as a cell suspension (d: *n=3*; triplicate samples) and at day 7 of culture (e: *n=4*; quadruplicate samples). *** $P < 0.001$. FBS = 15% FBS in DMEM. *Samples were normalized to de-epithelialized intestine. Error bars, s.d.

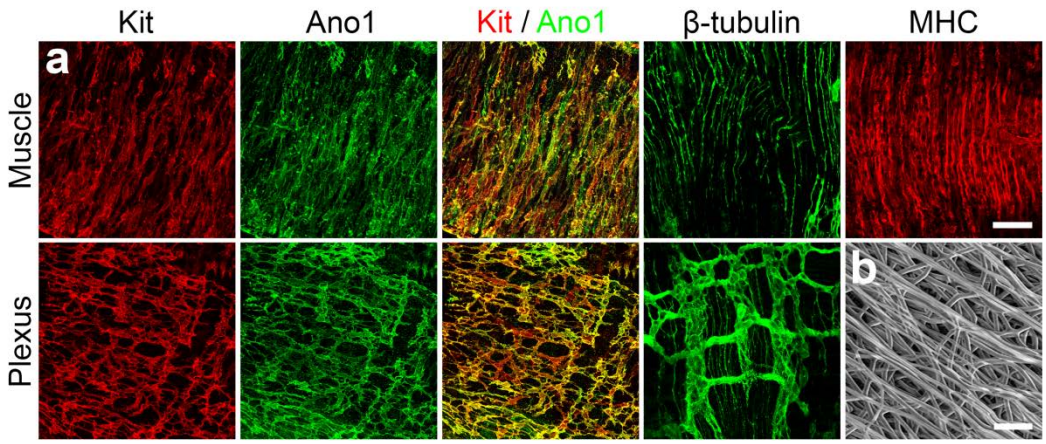

Supplementary Figure 3 | Cell alignment in the native murine small intestine. (**a**) Confocal images of immunofluorescent murine muscle strips with ICC markers showing co-localization (yellow) of Kit (red) and Ano1 (green), neuronal marker β-tubulin (green) and SMCs marker MHC (red). Scale bar, 50 μm. (**b**) Scanning electron micrographs of ePCL scaffold. The fiber alignment of ePCL scaffold was used to induce cell alignment. Scale bar, 25 μm. Muscle = muscle layer of murine small intestine. Plexus = myenteric plexus of murine small intestine.

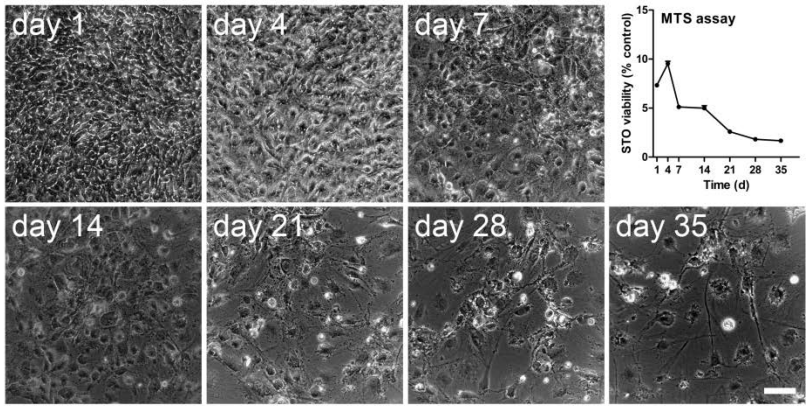

Supplementary Figure 4 | Viability of mitomycin C treated STO cells *in vitro* over time. 100k STO cells were cultured under the same conditions as with ISMC Mix co-culture. Cells were seeded on gelatin in STO medium overnight and cultured in FBS medium for 4 days followed by F12 medium. Phase contrast images and MTS assay measurements (*n=3*; triplicate samples; error bars, s.d.) were taken at each time point. Scale bar, 100 μm. F12 = advanced DMEM/F12.

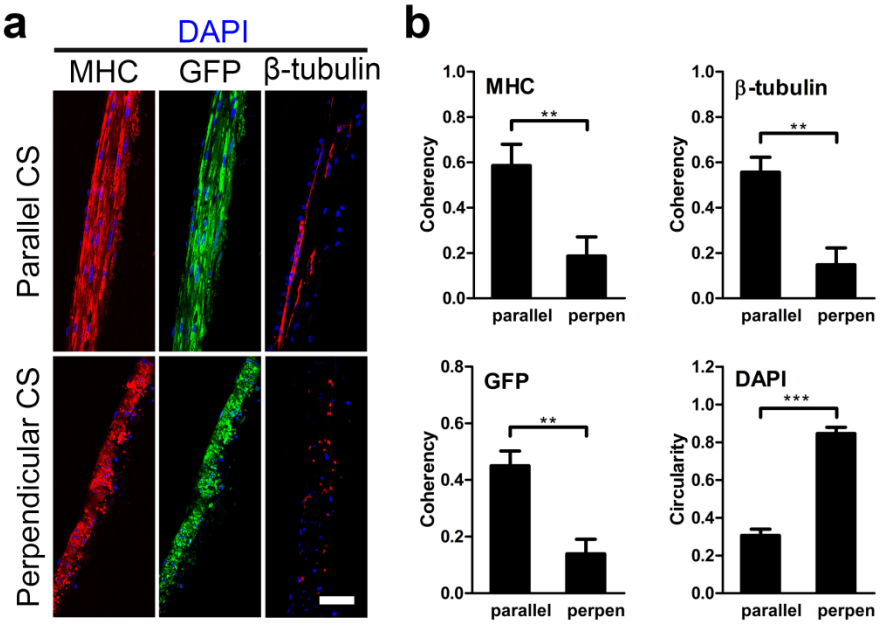

Supplementary Figure 5 | Alignment quantification of infiltrated ISMC Mix inside ePCL scaffolds at 10 weeks. Non-sorted cells from enzymatically digested intestinal muscle strips, ISMC Mix, were cultured on STO-seeded ePCL scaffolds. 100k ISMC Mix were cultured in FBS medium for the first 4 days before changing to F12 medium. ePCL scaffolds were cut in two orthogonal planes to expose cross section (CS) parallel or perpendicular (perpen) to ePCL's aligned fibers. (**a**) Confocal images of immunostained ISMC Mix with SMCs marker MHC (red), GFP (green), neuronal marker β-tubulin (red), and nuclear marker DAPI (blue) in parallel and perpendicular cross sections. Scale bar, 50 μm. (**b**) Coherency analysis (MHC, GFP and β-tubulin) and circularity analysis (DAPI) of infiltrated ISMC Mix inside ePCL scaffolds ($n = 3$). Coherency analysis = range from 0 (perfect random) to 1 (perfect alignment) indicating cell alignment. Circularity analysis = range from 0 (most elongated shape) to 1 (perfect circle) indicating elongation of nuclei due to cell alignment. *Samples were normalized to de-epithelialized intestine. Error bars, s.d. *** $P < 0.0001$, ** $P < 0.01$.

```
function multiROI()

[filename,filepath,~] = uigetfile('*.*',  'All Files (*.*)');

video_handle = VideoReader(fullfile(filepath, filename));

reference_frame = read(video_handle, 1);
frame_num = video_handle.NumberOfFrames;

% compute an average intensity change map
average_intensity_change = zeros(video_handle.Height, video_handle.Width);
for frame_idx = 1 : frame_num
    curr_frame = read(video_handle, frame_idx);
    average_intensity_change = average_intensity_change +
im2double(curr_frame(:, :, 2));
end
average_intensity_change = average_intensity_change ./ frame_num;


%figure(1), subplot(121); imshow(reference_frame);
figure(1), imagesc(average_intensity_change); axis image;

roi_num =input('Input the number of ROIs you want to select in this video:');
roi_masks = cell(roi_num, 1);
roi_images = cell(roi_num, 1);

for roi_idx = 1 : roi_num
    message = sprintf('%d out of %d ROI. Left click and hold to begin
drawing.\nSimply lift the mouse button to finish',...
        roi_idx, roi_num);
    uiwait(msgbox(message));
    hFH = imfreehand();
    roi_masks{roi_idx} = hFH.createMask();
    pos = hFH.getPosition();

    % define bounding box
    x1 =  max(1, min(round(min(pos(:,2))), video_handle.Height));
    y1 =  max(1, min(round(min(pos(:,1))), video_handle.Width));
    x2 =  max(1, min(round(max(pos(:,2))), video_handle.Height));
    y2 =  max(1, min(round(max(pos(:,1))), video_handle.Width));

    roi_image_r = reference_frame(:, :, 1) .* uint8(roi_masks{roi_idx});
    roi_image_g = reference_frame(:, :, 2) .* uint8(roi_masks{roi_idx});
    roi_image_b = reference_frame(:, :, 3) .* uint8(roi_masks{roi_idx});
    roi_images{roi_idx} = cat(3, ...
        roi_image_r(x1:x2, y1:y2), ...
        roi_image_g(x1:x2, y1:y2), ...
        roi_image_b(x1:x2, y1:y2));
end

fprintf('Start processing.\n');
average_intensity = zeros(frame_num, roi_num);
average_interval = 1.0 / video_handle.FrameRate;
```

```
for i = 1 : frame_num
    raw_frame = read(video_handle, i);
    green_channel = double(raw_frame(:, :, 2));
    % abandon red and blue channel, because mostly no data is available
    for roi_idx = 1 : roi_num
        average_intensity(i, roi_idx) =
mean(green_channel(roi_masks{roi_idx}));
    end
end

% filter out the first dark period
thres = mean(average_intensity) - 3 * std(average_intensity);

valid_frame_indices = zeros(roi_num, 1);
for roi_idx = 1 : roi_num
    indices = sort(find(average_intensity(:, roi_idx) >= thres(roi_idx)),
'ascend');
    valid_frame_indices(roi_idx) = indices(1);
end

for roi_idx = 1 : roi_num
    figure; hold on;
    title(sprintf('ROI %d', roi_idx));
    subplot(231); imagesc(roi_images{roi_idx}(:, :, 2)); axis image;
title(sprintf('Image ROI %d', roi_idx));
    axis off;

    truncated_average_intensity =
average_intensity(valid_frame_indices(roi_idx):end, roi_idx) %; want to know
this number
    truncated_timestamps = [valid_frame_indices(roi_idx) : frame_num] .*
average_interval;

    truncated_timestamps'

    Y = fft(truncated_average_intensity);
    n=length(Y);
    Y=Y(1:ceil(n/2));
    n=length(Y);
    mY=abs(Y);

    subplot(233); hold on;
    FREQ=(0:n-1)*(video_handle.FrameRate /(2*n));
    semilogy(FREQ, mY);
    xlabel('Frequency (Hz)');
    title('Periodogram of Depolarization');

    subplot(232); hold on;
    xlabel('Time (seconds)');
    ylabel('Intensity (percent)');
    title('Mean Intensity Over Time');

    plot(truncated_timestamps, truncated_average_intensity);
```

```
    % Establish characteristics of the FFT (Periodogram) of the intensity
plot
    % of depolarizing cells.  This plot is the top right image.

    % I also create a zero-centered Periodogram for easier visualization.
This
    % plot is on the bottom left figure.
    Z=fftshift(mY);
    f0 = (-n/2:n/2-1)*.5*(video_handle.FrameRate/(length(Y)));  % 0-centered
frequency range
    subplot(235); hold on;
    plot(f0,Z);
    xlabel('Frequency (Hz)');
    title('Zero-shift Periodogram of Depolarization');

    [pks,locs] = findpeaks(Z);
    [pkvals,idx] = sort(pks,'descend'); %sort to vector
    pkvals(2); %second largest value - the first is always 0 and doesn't mean
anything
    index=find(Z==pkvals(2));
    mainFrequencyStr=num2str(f0(index));
    plot(f0(index),Z(index),'r.', 'MarkerSize',25);
    text(f0(index),Z(index),['Frequency = ',mainFrequencyStr, ' Hz']);
    Frequency = f0(index);
    axis([0 ceil(10*f0(index)) 0 ceil(2*pkvals(2))]);
    fprintf('ROI %d: Frequency %f Hz\n', roi_idx, f0(index));

    % I do the same thing for the inverse of the frequency, aka the period.
    period=1./FREQ;
    subplot(236); hold on;
    plot(period,mY);
    [pks2,locs2] = findpeaks(mY);
    [pkvals2,idx2] = sort(pks2,'descend'); %sort to vector
    pkvals2(1); % largest value
    index2=find(mY==pkvals2(1));
    mainPeriodStr=num2str(period(index2));
    plot(period(index2),mY(index2),'r.', 'MarkerSize',25);
    text(period(index2),mY(index2),['Period = ',mainPeriodStr, ' Seconds']);
    xlabel('Period (seconds)');
    axis([0 ceil(2*period(index2)) 0 ceil(2*pkvals2(1))]);
    fprintf('ROI %d: Period %f seconds.\n', roi_idx, period(index2));
end
end
```

Supplementary Figure 6 | Matlab code for analyzing Ca^{2+} oscillation videos. Multiple regions of interest (ROIs) can be selected and the average fluorescent intensity within the selected regions is calculated for each frame. Outputs include time-course change in fluorescence intensity, frequency and period for each selected ROI.

```
%Reset everything
clear all;
close all;

bordervector = [0 16 30 34 48 64];
colorscale=zeros(64,3);

for j=1:64
    if bordervector(1)<=j && j<=bordervector(2)
        colorscale(j,1)=0;
        colorscale(j,2)=0;
        colorscale(j,3)=1;
    end

    if bordervector(2)<j && j<=bordervector(3)
        scale1=((j-15)*18)/270;
        colorscale(j,1)=scale1;
        colorscale(j,2)=scale1;
        colorscale(j,3)=1;
    end

    if bordervector(3)<j && j<=bordervector(4)
        colorscale(j,:)=1;
    end

    if bordervector(4)<j && j<=bordervector(5)
        scale2=(255-((j-34)*18))/255;
        colorscale(j,1)=1;
        colorscale(j,2)=scale2;
        colorscale(j,3)=scale2;
    end

    if bordervector(5)<j && j<=bordervector(6)
        colorscale(j,1)=1;
        colorscale(j,2)=0;
        colorscale(j,3)=0;
    end
end

% Note: a large portion of this code was directly taken and modified
% from code used in "Smooth muscle strips for intestinal tissue engineering"
% by Chris Walthers.

%Ask user to choose a file to run.  This should be a .wmv file.  If it is
%not, you can easily convert with Windows Live Movie Maker
[FileName,PathName,filterindex] = uigetfile('*.*',  'All Files (*.*)');

%The following allows you to shorten the video produced by this code.
framenum=input('How many frames do you want to skip between each frame
captured? (Must be greater than 0)  ');
fps=30; %frames per second; wmvs are always 30
sample=fps/(framenum); %establish how many frames per second new video will
have, important for the FFT part
```

```
% Saves the new video in the same folder as the input video
outputFolder = PathName;

% Read in the movie.
mov = VideoReader(FileName);
new_FileName = strrep(FileName, '.wmv', '_CAcode_output');

% Determine how many frames there are, and pixels, and final number of
% frames
nFrames = mov.NumberOfFrames;
videoHeight = mov.Height;
videoWidth = mov.Width;
newframes=floor(nFrames/(framenum+1));

% Preallocate movie structure.
movie1(1:newframes) = struct('cdata', zeros(videoHeight, videoWidth, 3,
'uint8'), 'colormap', []);

% % Read one frame at a time.
for k = 1 : newframes
    movie1(k).cdata = read(mov, k*(framenum+1)-framenum+1);
end

%Preallocate structure for subsequent structures
greendata=zeros(videoHeight,videoWidth,newframes);
subtracted=zeros(videoHeight,videoWidth,(newframes-1));

for l=1:newframes
greendata(:,:,l)=movie1(l).cdata(:,:,2);
end

% Display the freehand mask in a 6 panel window with some cool extra figures
figure('units','normalized','outerposition',[0 0 1 1]);
workspace;  % Make sure the workspace panel is showing.
fontSize = 16;

% colormap(colorscale);
% colormap jet;
colormap gray;
colormap(flipud(colormap));
% colormap(flipud(colormap));
%Do some housekeeping

clear movie1;

% Prepare the new video file.
% New file will have same file name as before, but with _CAcodeFFT.avi at
% the end.
% vidObj = VideoWriter(new_FileName,'Uncompressed AVI');
vidObj = VideoWriter(new_FileName,'Motion JPEG AVI');
open(vidObj);
```

```
% This is a "for loop" that subtracts the first image in the video from all
% subsequent images.  In effect, this "normalizes" every frame of the video
% to the first frame (arbitrarily... you could do the same with any frame
% from the video for similar effect).  Now the new video will show changes
% in intensity from the first frame.
% colormap(colorscale);


for m=2:newframes
subtracted(:,:,m)=imsubtract(greendata(:,:,m), greendata(:,:,3));
image((subtracted(:,:,m))+31);
currFrame=getframe;
writeVideo(vidObj,currFrame);
end

% This line makes it easier to view stills from your video exactly as they
% appear in the video
subtracted=subtracted+31;

% % % This code plays a series of stills for reviewing your video after
% making it
% % selectImage = implay(subtracted);
% % selectImage.Visual.ColorMap.UserRangeMin=0;
% % selectImage.Visual.ColorMap.UserRangeMax=64;
% % selectImage.Visual.ColorMap.UserRange = 1;
% % set(findall(0,'tag','spcui_scope_framework'),'position',[100 150
(videoWidth)*1.1 (videoHeight)*1.1]);

% Close the file.
close(vidObj);
% Housekeeping
% clear greendata; clear subtracted;
```

Supplementary Figure 7 | Matlab code for processing Ca^{2+} oscillation videos. Original video can be condensed by capturing only every nth frame (every 3th frame was used to produce supplementary video 1). The intensity values from the first frame in the video are subtracted as baseline intensity from each subsequent frame to create a normalized intensity profile compared to the first frame. Changes in fluorescent intensity, corresponding to calcium concentration, are color-mapped to show in grayscale with an increase in black, decrease in white, or no change in gray relative to the first frame.

3.9 SUPPLEMENTARY VIDOES

Supplementary Video 1 | Ca^{2+} oscillation of ICC in the culture of MACS+ cells on STO at day 7. The original video was processed with matlab so that it is about three times faster than the real time and color normalized to the first frame of the video, where higher intensity shows up lighter and lower intensity shows up darker.

Supplementary Video 2, 3 | ISMC Mix without GFP expression (**2**) and with GFP expression (**3**) cultured on STO cells *in vitro* for a week.

Supplementary Video 4 | ISMC Mix were cultured on STO cells seeded ePCL scaffolds for 8 weeks.

3.10 REFERENCE

1. Bines, J. E. Intestinal failure: A new era in clinical management. *J. Gastroenterol. Hepatol.* **24,** S86–S92 (2009).
2. Donohoe, C. L. & Reynolds, J. V. Short bowel syndrome. *Surgeon* **8,** 270–9 (2010).
3. Sato, T. *et al.* Single Lgr5 stem cells build crypt–villus structures in vitro without a mesenchymal niche. *Nature* **459,** 262–265 (2009).
4. Sala, F. G., Kunisaki, S. M., Ochoa, E. R., Vacanti, J. & Grikscheit, T. C. Tissue-Engineered Small Intestine and Stomach Form from Autologous Tissue in a Preclinical Large Animal Model. *J. Surg. Res.* **156,** 205–212 (2009).
5. Jain, R. K., Au, P., Tam, J., Duda, D. G. & Fukumura, D. Engineering vascularized tissue. *Nat. Biotechnol.* **23,** 821–823 (2005).
6. L'Heureux, N. *et al.* Human tissue-engineered blood vessels for adult arterial revascularization. *Nat. Med.* **12,** 361–365 (2006).
7. Ott, H. C. *et al.* Perfusion-decellularized matrix: using nature's platform to engineer a bioartificial heart. *Nat. Med.* **14,** 213–221 (2008).
8. Engelmayr, G. C. *et al.* Accordion-like honeycombs for tissue engineering of cardiac anisotropy. *Nat. Mater.* **7,** 1003–1010 (2008).
9. Radisic, M., Marsano, A., Maidhof, R., Wang, Y. & Vunjak-Novakovic, G. Cardiac tissue engineering using perfusion bioreactor systems. *Nat. Protoc.* **3,** 719–38 (2008).
10. Laflamme, M. A. & Murry, C. E. Regenerating the heart. *Nat. Biotechnol.* **23,** 845–856 (2005).

11. Camargo, F. D., Green, R., Capetenaki, Y., Jackson, K. A. & Goodell, M. A. Single hematopoietic stem cells generate skeletal muscle through myeloid intermediates. *Nat. Med.* **9,** 1520–1527 (2003).

12. Walthers, C. M., Lee, M., Wu, B. M. & Dunn, J. C. Y. Smooth muscle strips for intestinal tissue engineering. *PLoS One* **9,** e114850 (2014).

13. Lee, M., Wu, B. M., Stelzner, M., Reichardt, H. M. & Dunn, J. C. Y. Intestinal smooth muscle cell maintenance by basic fibroblast growth factor. *Tissue Eng. Part A* **14,** 1395–402 (2008).

14. Sanders, K. M., Koh, S. D., Ro, S. & Ward, S. M. Regulation of gastrointestinal motility--insights from smooth muscle biology. *Nat. Rev. Gastroenterol. Hepatol.* **9,** 633–45 (2012).

15. Sanders, K. A case for interstitial cells of Cajal as pacemakers and mediators of neurotransmission in the gastrointestinal tract. *Gastroenterology* **111,** 492–515 (1996).

16. Sanders, K. M., Koh, S. D. & Ward, S. M. Interstitial cells of cajal as pacemakers in the gastrointestinal tract. *Annu. Rev. Physiol.* **68,** 307–43 (2006).

17. Langton, P., Ward, S. M., Carl, A., Norell, M. A. & Sanders, K. M. Spontaneous electrical activity of interstitial cells of Cajal isolated from canine proximal colon. *Proc. Natl. Acad. Sci.* **86,** 7280–7284 (1989).

18. Zhu, M. H. *et al.* A Ca(2+)-activated Cl(-) conductance in interstitial cells of Cajal linked to slow wave currents and pacemaker activity. *J. Physiol.* **587,** 4905–18 (2009).

19. Huizinga, J. D. *et al.* W/kit gene required for interstitial cells of Cajal and for intestinal pacemaker activity. *Nature* 347–349 (1995).

20. Klüppel, M., Huizinga, J. D., Malysz, J. & Bernstein, A. Developmental origin and Kit-dependent development of the interstitial cells of cajal in the mammalian small intestine. *Dev. Dyn.* **211,** 60–71 (1998).

21. Liu, L. W., Thuneberg, L. & Huizinga, J. D. Development of pacemaker activity and interstitial cells of Cajal in the neonatal mouse small intestine. *Dev. Dyn.* **213,** 271–82 (1998).

22. Maeda, H., Yamagata, A., Nishikawa, S. & Yoshinaga, K. Requirement of c-kit for development of intestinal pacemaker system. *Development* **116,** 369–375 (1992).

23. Wu, J. J., Rothman, T. P. & Gershon, M. D. Development of the interstitial cell of Cajal: origin, kit dependence and neuronal and nonneuronal sources of kit ligand. *J. Neurosci. Res.* **59,** 384–401 (2000).

24. Torihashi, S. *et al.* Blockade of kit signaling induces transdifferentiation of interstitial cells of Cajal to a smooth muscle phenotype. *Gastroenterology* **117,** 140–148 (1999).

25. Thomson, L. *et al.* Interstitial cells of Cajal generate a rhythmic pacemaker current. *Nat. Med.* **4,** 848–851 (1998).

26. Koh, S. D., Sanders, K. M. & Ward, S. M. Spontaneous electrical rhythmicity in cultured interstitial cells of Cajal from the murine small intestine. *J. Physiol.* **513,** 203–213 (1998).

27. Rumessen, R. I. J. Interstitial Cells of Cajal in Human Gut and Gastrointestinal Disease. *Microsc. Res. Tech.* **47,** 344–360 (1999).

28. Sanders, K. M., Ordög, T. & Ward, S. M. Physiology and pathophysiology of the interstitial cells of Cajal: from bench to bedside. IV. Genetic and animal models of GI motility disorders caused by loss of interstitial cells of Cajal. *Am. J. Physiol. Gastrointest. Liver Physiol.* **282,** G747–56 (2002).

29. Burns, A. J. Disorders of interstitial cells of Cajal. *J. Pediatr. Gastroenterol. Nutr.* **45 Suppl 2,** S103–6 (2007).

30. Farrugia, G. Interstitial cells of Cajal in health and disease. *Neurogastroenterol. Motil.* **20,** 54–63 (2008).

31. Talbot, N. C., Sparks, W. O., Powell, A. M., Kahl, S. & Caperna, T. J. Quantitative and semiquantitative immunoassay of growth factors and cytokines in the conditioned medium of STO and CF-1 mouse feeder cells. *In Vitro Cell. Dev. Biol. Anim.* **48,** 1–11 (2012).

32. Kobayashi, M., Lei, N. Y., Wang, Q., Wu, B. M. & Dunn, J. C. Y. Orthogonally oriented scaffolds with aligned fibers for engineering intestinal smooth muscle. *Biomaterials* **61,** 75–84 (2015).

33. Gomez-Pinilla, P. J. *et al.* Ano1 is a selective marker of interstitial cells of Cajal in the human and mouse gastrointestinal tract. *Am. J. Physiol. Gastrointest. Liver Physiol.* **296,** G1370–81 (2009).

34. Chen, Y. *et al.* Visualization of the interstitial cells of cajal (ICC) network in mice. *J. Vis. Exp.* 3–7 (2011). doi:10.3791/2802

35. Komuro, T. Structure and organization of interstitial cells of Cajal in the gastrointestinal tract. *J. Physiol.* **576,** 653–8 (2006).

36. Ordög, T., Redelman, D., Horowitz, N. N. & Sanders, K. M. Immunomagnetic enrichment of interstitial cells of Cajal. *Am. J. Physiol. Gastrointest. Liver Physiol.* **286,** G351–60 (2004).

37. Torihashi, S., Fujimoto, T., Trost, C. & Nakayama, S. Calcium oscillation linked to pacemaking of interstitial cells of Cajal: requirement of calcium influx and localization of TRP4 in caveolae. *J. Biol. Chem.* **277,** 19191–7 (2002).

38. Ishikawa, T. *et al.* Characterization of in vitro gutlike organ formed from mouse embryonic stem cells. *Am. J. Physiol. Cell Physiol.* **286,** C1344–52 (2004).

39. Lee, J. *et al.* Neurotensin modulates pacemaker activity in interstitial cells of Cajal from the mouse small intestine. *Mol. Cells* **33,** 509–16 (2012).

40. Lee, J. C. F. *et al.* Generation of slow waves in membrane potential is an intrinsic property of interstitial cells of Cajal Generation of slow waves in membrane potential is an intrinsic property of interstitial cells of Cajal. *Am. J. Physiol. Gastrointest. Liver Physiol.* **277,** G409–23 (1999).

41. Ward, S. M. *et al.* Rapid Report Pacemaking in interstitial cells of Cajal depends upon calcium handling by endoplasmic reticulum and mitochondria. 355–361 (2000).

42. Nair, D. G. *et al.* Proliferation modulates intestinal smooth muscle phenotype in vitro and in colitis in vivo. *Am. J. Physiol. Gastrointest. Liver Physiol.* **300,** G903–13 (2011).

43. Liang, J. *et al.* The C-kit receptor-mediated signal transduction and tumor-related diseases. *Int. J. Biol. Sci.* **9,** 435–43 (2013).

44. Roskoski, R. Signaling by Kit protein-tyrosine kinase--the stem cell factor receptor. *Biochem. Biophys. Res. Commun.* **337,** 1–13 (2005).

45. Drumm, B. T., Koh, S. D., Andersson, K.-E. & Ward, S. M. Calcium signalling in Cajal-like interstitial cells of the lower urinary tract. *Nat. Rev. Urol.* **11,** 555–64 (2014).

46. Geisbauer, C. L., Chapin, J. C., Wu, B. M. & Dunn, J. C. Y. Transplantation of Enteric Cells Expressing p75 in the Rodent Stomach. *J. Surg. Res.* **174,** 257–65 (2012).

47. Zeng, S., Li, B., Zeng, S. & Chen, S. Simulation of spontaneous Ca2+ oscillations in astrocytes mediated by voltage-gated calcium channels. *Biophys. J.* **97,** 2429–37 (2009).

48. Daniel, E. E., Boddy, G., Bong, A. & Cho, W. A new model of pacing in the mouse intestine. *Am. J. Physiol. Gastrointest. Liver Physiol.* **286,** G253–62 (2004).

49. Khalil, H. A. *et al.* Mouse model of endoscopically ablated enteric nervous system. *J. Surg. Res.* (2015). doi:10.1016/j.jss.2015.07.034

CHAPTER FOUR: CONCLUSIONS AND FUTURE DIRECTIONS

4.1 IDENTIFY A FEEDER-FREE CULTURE SYSTEM FOR INTESTINAL SMOOTH MUSCLE ENGINEERING

The objective of this project was to identify the culture system to maintain functional ICC for functional smooth muscle tissue engineering. This was achieved by using a feeder layer culture system with standard medium (Chapter 3). However, it is ideal to pursue a feeder-free culture system for the intestinal tissue engineering purpose. In order to achieve this goal, the following two aspects were considered: 1) what STO cells were secreting into the medium, which lead to media optimization, and 2) what STO cells were expressing on the cell surface, which lead to substrate optimization.

4.1.1Media optimization: necessity of STO cells conditioned media?

STO cells are known to secret many factors and commonly used for *in vitro* maintenance and growth of embryonic stem cells and induced pluripotent stem cells. Examples of growth factors abundantly present in conditioned medium of the STO cells (STO-CM) are activin A, insulin-like growth factor 1(IGF-1), insulin-like growth factor 2(IGF-2), macrophage colony-stimulating factor (M- CSF), and pigment epithelium-derived factor (PEDF), but particularly more hepatocyte growth factor (HGF), and SCF[1]. Also, it should be noted that STO cells lacks expression of EGF and FGF family members[1]. We already showed that exogenous addition of SCF failed to support ICC growth any better (with higher ICC seeding density at 60k), and that STO-CM was only helpful to increase Kit expression of ICC culture with lower seeding density at 15k but not with higher seeding density at 60k (Chapter 3). Therefore, the effect of STO-CM for ISMC Mix containing ICC, SMC and neuronal cells might be also limited. Yet, it is worth

investigating as a part of effort to achieve feeder-free culture system because there are cases in which conditioned media is effective. For example, previous work in our group demonstrated that intestinal subepithelial myofibroblasts conditioned media enhanced the growth of intestinal crypts[2].

In preliminary experiments, the STO media (Chapter 3) was replaced about one day after mytomycin C treatment of confluent STO monolayer. The F12 medium (Chapter 3) was collected after 3~4 days of incubation, passed through a 0.2 mm pore size filter, and used as STO-CM stock. The cell cultures grown with STO-CM were given media composed of STO-CM stock and the fresh F12 medium (Chapter 3) in a 1:1 ratio. When ISMC Mix (Chapter 3) were grown on gelatin, the improvement made by STO-CM in ICC marker Kit and Ano1 colocalization, SMCs marker MHC, and neuronal marker β-tubulin was obvious compared to FBS medium (Chapter 3), yet not noticeable compared to F12 medium. The STO cells were much more effective in preserving the ICC population within the ISMC Mix culture by securing not only ICC but also other types of cell attachment, and soluble factors in STO-CM could not meet the level of the effectiveness of STO cells. Therefore, the necessity of STO-CM when F12 medium is used as base medium is currently under investigation. These preliminary results of STO-CM lead us to investigate in optimizing a substrate for better cell attachment and initial cell survival.

4.1.2 Substrate optimization: SCF immobilized ePCL scaffolds

SCF exists as two distinct isoforms of transmembrane proteins expressed on the cell surface[3]. Soluble SCF (sSCF) undergoes rapid proteolytic cleavage and release from the plasma membrane, while membrane-bound SCF (mSCF) releases sSCF much more slowly due to the

lack of the proteolytic cleavage site[4]. Consequently, both isoforms originally exist as mSCF and the main difference is the rate of cleavage and release of biologically active sSCF. Both isoforms seem to play a specific physiological role because the ratio of the two varies in different tissues[3]. It was found that mutant mice only expressing sSCF but no mSCF failed to exhibit a spontaneous, rhythmic electrical slow wave, and ICC-MY were absent in the myenteric plexus [5,6]. This suggests that mSCF may have a crucial role for the development and maintenance of ICC-MY. In addition, stimulation of Kit with mSCF in Mo7E (SCF-dependent myeloid cell line) activated Kit receptor more persistently than stimulation with sSCF [7]. Therefore, mSCF may activate Kit on ICC more effectively than sSCF. A previous study demonstrated that a SCF immobilized substrate supported the proliferation of Mo7E cells[8]. To my knowledge, no one has developed a suitable scaffold that can induce functional ICC and SMC proliferation and/or maturation. Since feeder cells used in our ICC culture system may not be compatible with the host animal/patient, it will be critical to develop implantable scaffolds to support ICC proliferation and maturation for intestinal muscle engineering.

In preliminary experiments, ePCL scaffolds were used to induce ICC and SMC alignment and network formation. In order to mimic mSCF, SCF were immobilized on the surface of ePCL by using sulfo-sanpah chemistry, which was the same procedure used to improve the hydrophilicity of a PDMS surface[9]. Several surface treatments of ePCL tested include plasma etching[10] (plasma-ePCL), UV irradiation[11] (UV-ePCL), (3-Aminopropyl)triethoxysilane (APTS) conjugation (NH_2-ePCL), sulfo-sanpah conjugation (COOH-ePCL), SCF conjugation (mSCF-ePCL), and gelatin coating. Plasma etching (air plasma for 1min) was very effective in making ePCL hydrophilic for later sulfo-sanpah conjugation containing strong UV irradiation in its procedure and for gelatin coating. Unfortunately, there was no noticeable difference in cell

attachment and ICC markers Kit and Ano1 expressions among MACS+ cells seeded on mSCF-ePCL, COOH-ePCL and NH_2-ePCL. The effort of improving SCF conjugation procedure by increasing the concentration of SCF solution from 1ug/ml to 10ug/ml and adding the SCF solution right after the sulfo-sanpah conjugation to the ePCL failed to enhance ISMC Mix attachment to mSCF-ePCL compared to plasma-UV-ePCL, COOH-ePCL and NH_2-ePCL.

According to previous studies, Kit receptor dimerization is necessary for effective activation of protein kinase activity and its downstream signaling pathway for ICC development. Also, the non-covalent homodimeric form of SCF stimulates cell growth more effectively than monomeric SCF [12,13]. In order to make mSCF-ePCL effective for ICC attachment and proliferation, not only the amount but also the orientation and formation of SCF conjugated to the ePCL may matter. Ideally, ePCL with enough homodimeric SCF immobilizion with its Kit binding site exposed should effectively activate Kit receptor dimerization for ICC to survive. Therefore, many factors still need to be considered for the substrate optimization.

4.2 CONCLUDING REMARKS

Although the media and substrate optimization efforts alone have not shown conclusive results, the combination of the two optimized system might bring some synergetic effect in improving not only ICC but also the whole ISMC Mix attachment and survival *in vitro*. Yet, the media and substrate optimization we mentioned above is all about chemical stimulation. We also need to consider the effect of mechanical stimulation on functional intestinal tissue engineering as a whole. For example, application of mechanical stress is known to induce mature phenotype of SMC, including higher MHC expression. Not only can a bioreactor with an automated program impose mechanical stress on seeded cells, but also the substrate with varying stiffness can have a

significant effect. If our purpose is to induce higher MHC expression of SMC, the stiffer the substrate is the more effective it is. However, we have to keep in mind that in order to bioengineer functional intestinal smooth muscle, SMC as well as all the other types of cells including ICC and neuronal cells in the ISMC Mix need to be functional and mature. In contrast to SMC, it is well known that neuronal cells survive and mature better on softer substrates. Therefore, there should be an optimal substrate stiffness for ISMC Mix culture as a whole entity.

The STO cells proved its ability to maintain not only ICC but also SMC populations functional (Chapter 3). The in-depth investigation of why and how the STO culture system enables the engineering of ISMC Mix into functional smooth muscle with spontaneous rhythmic contraction *in vitro* might give us the missing puzzle pieces to overcome challenges in the current optimization for achieving the feeder-free culture system. If people with a deep understanding of biomaterial, bioconjugation and molecular biology work hard together to solve the puzzle, the feeder-free implant that mimics interstitial smooth muscle structurally and functionally should be accomplished in near future. Finally, the knowledge gained in bioengineering functional intestinal smooth muscle should be widely applicable to other types of smooth muscle in other visceral organs, contributing to the entire tissue engineering and regenerative medicine field to move forward.

4.3 REFERENCES

1. Talbot, N. C., Sparks, W. O., Powell, A. M., Kahl, S. & Caperna, T. J. Quantitative and semiquantitative immunoassay of growth factors and cytokines in the conditioned medium of STO and CF-1 mouse feeder cells. *In Vitro Cell. Dev. Biol. Anim.* **48,** 1–11 (2012).
2. Lei, N. Y. *et al.* Intestinal subepithelial myofibroblasts support the growth of intestinal epithelial stem cells. *PLoS One* **9,** e84651 (2014).
3. Huang, E. J., Nocka, K. H., Buck, J. & Besmer, P. Differential expression and processing of two cell associated forms of the kit-ligand: KL-1 and KL-2. *Mol. Biol. Cell* **3,** 349–62 (1992).
4. Pandiella, A., Bosenberg, M. W., Huang, E. J., Besmer, P. & Massagué, J. Cleavage of membrane-anchored growth factors involves distinct protease activities regulated through common mechanisms. *J. Biol. Chem.* **267,** 24028–33 (1992).
5. Broudy, V. C. Stem cell factor and hematopoiesis. *Blood* **90,** 1345–64 (1997).
6. Ward, S. M., Burns, A. J., Torihashi, S., Harney, S. C. & Sanders, K. M. Impaired development of interstitial cells and intestinal electrical rhythmicity in steel mutants. *Am. J. Physiol.* **269,** C1577-85 (1995).
7. Miyazawa, K. *et al.* Membrane-bound Steel factor induces more persistent tyrosine kinase activation and longer life span of c-kit gene-encoded protein than its soluble form. *Blood* **85,** 641–9 (1995).
8. Alberti, K. *et al.* Functional immobilization of signaling proteins enables control of stem cell fate. *Nat. Methods* **5,** 645–650 (2008).
9. Pushkarsky, I. *et al.* Automated single-cell motility analysis on a chip using lensfree microscopy. *Sci. Rep.* **4,** 4717 (2014).

10. Hegemann, D., Brunner, H. & Oehr, C. Plasma treatment of polymers for surface and adhesion improvement. *Nucl. Instruments Methods Phys. Res. Sect. B Beam Interact. with Mater. Atoms* **208,** 281–286 (2003).

11. Li, B., Ma, Y., Wang, S. & Moran, P. M. A technique for preparing protein gradients on polymeric surfaces: effects on PC12 pheochromocytoma cells. *Biomaterials* **26,** 1487–95 (2005).

12. Liang, J. *et al.* The C-kit receptor-mediated signal transduction and tumor-related diseases. *Int. J. Biol. Sci.* **9,** 435–43 (2013).

13. Roskoski, R. Signaling by Kit protein-tyrosine kinase--the stem cell factor receptor. *Biochem. Biophys. Res. Commun.* **337,** 1–13 (2005).